HIGH-ENERGY ULTRAFAST YTTERBIUM FIBER LASERS

A Dissertation

Presented to the Faculty of the Graduate School

of Cornell University

In Partial Fulfillment of the Requirements for the Degree of

Doctor of Philosophy

by

Joel Buckley

August 2006

HIGH-ENERGY ULTRAFAST YTTERBIUM FIBER LASERS

Joel Buckley, Ph. D.

Cornell University 2006

Within the past two decades, applications for sources of ultrafast pulses of optical radiation have expanded beyond the confines of research laboratories. Applications are too numerous to list in entirety but include uses in the fields of medicine, micromachining, high-bit-rate telecommunications, optical range-finding, and detection of trace chemicals to name a few. Currently, the market is dominated by femtosecond solid-state lasers due to their superior pulse energy and quality. However, many sources are being replaced with fiber-based lasers due to their inherent stability, compact design, and reduced cost. Moreover, fiber lasers have excellent beam quality and are easily scalable to high average powers.

This thesis summarizes research on femtosecond ytterbium-doped (Yb) fiber lasers operating in the near-infrared spectrum (~ 1-micron wavelength). There is strong interest for stable, femtosecond sources at this wavelength for biomedical imaging and noninvasive surgery. The overriding theme of this research is an attempt to better understand the limitations of short-pulse fiber lasers, with the goal of providing higher-energy, shorter-duration, and higher-quality optical pulses from fiber.

In the context of high energy, two approaches are reviewed. In the first approach, fiber nonlinearities are exploited through relatively new forms of pulse evolution which provide stable, high-power operation. In the second approach, excessive

nonlinearity is avoided as much as possible, and high-energy pulse formation is stabilized with an intra-cavity frequency filter. Experiments have successfully generated the highest pulse energy (3-times improvement), highest peak power (50% improvement), and highest average power from any fiber oscillator.

Also discussed is a new regime of modelocked operation for fiber lasers, which is referred to as chirped-pulse oscillation. In this regime, highly-chirped pulses are generated which are relatively unchanged during propagation in the laser. While these pulses suffer some in quality, they can attain relatively high energy and can be de-chirped external to the laser, achieving durations of a few hundred femtoseconds.

A fiber laser is explored which is capable of generating extremely short, high-quality pulses. By compensating for higher-order dispersion inside the oscillator, record pulse durations are generated with excellent pulse quality that is more typical of solid-state lasers.

Finally, an experiment is discussed in which a fiber laser is modelocked with a semiconductor saturable absorber mirror (SESAM). Femtosecond durations are achieved. This laser represents a first step toward an environmentally stable source of high-energy, short pulses.

BIOGRAPHICAL SKETCH

Joel Buckley was born in Houston, Texas in 1975 to Larry and Catherine Buckley. He spent the first half of his childhood living in a small town in Pennsylvania, and the second half living in an even smaller town in Missouri. Seclusion led to much contemplation, and Joel often wondered about the workings of the universe. Science fascinated him from an early age, and when it came time to leave home, he went off to the University of Missouri at Rolla to study physics. After receiving his B.S. degree, he began his Ph.D. studies in the department of Applied and Engineering Physics at Cornell University. It was there that he joined the Wise research group, engaging in the study of nonlinear and ultrafast optics. Four years later, and four decades wiser, Joel leaves Cornell greatly indebted to his advisor, his co-workers, and many others in the Ithaca community who have helped him along the way. He begins a new life in New Mexico, working for Sandia National Laboratories where he hopes to continue his tradition of burning things with lasers (but on a much larger scale).

To my wife Amy, for her constant inspiration

ACKNOWLEDGMENTS

I am very grateful to my advisor, Professor Frank Wise, who took me into his group four years ago and taught me through his words and actions what it means to practice science. From him, I have learned the importance of seeing the big picture as well as the virtues of patience and integrity. I will forever be in his debt. I am also grateful to Professor Gaeta and Professor Lipson who are my committee members, and who have never failed to assist me when I needed them. I thank Professor Lisa Wickham, for whom I worked as a teaching assistant one semester. Her door was always open for me, and I value our many discussions. I owe much to my co-workers in Wise group. When I first began my research, Ömer Ilday took me under his wing and often worked with me on a daily basis. Much of this thesis would not have been accomplished were it not for him. It has been a pleasure working with other members of the fiber laser team, including Hyungsik Lim, Andy Chong, Lyuba Kuznetsova, Shian Zhou, and more recently Will Renninger. Some of Will's simulations are presented alongside work in this thesis. Finally, I am indebted to my wife and family who have stood by me all these years.

TABLE OF CONTENTS

LIST OF FIGURES

Chapter 1

Introduction

1.1 General background for ultrafast lasers

A few years after the demonstration of the first laser in 1960, the first ultrafast optical pulses were generated [1]. Since this time, the generation and propagation of short optical pulses has grown into a scientific field of its own. Short pulses are created in a laser by locking together the longitudinal cavity modes (called modelocking). In active modelocking, a rapid shutter is used to force pulse formation inside the laser. Actively modelocked lasers can produce ~ 100-ps pulse durations or longer. Passive modelocking is achieved by setting the cavity conditions such that a pulse is the steady-state solution of the laser. In other words, a pulsed solution experiences lower intra-cavity loss than a continuous wave (CW) solution. This is achieved by introducing a saturable absorber (SA) into the laser cavity. The SA is an element which preferentially transmits higher intensities. Starting from noise, a pulse is shaped by an SA with each cavity round trip. A conceptual diagram is shown in Figure 1.1.

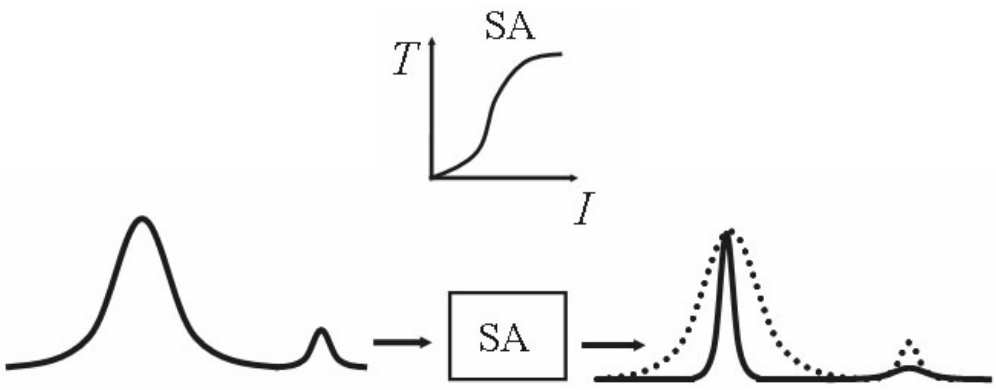

Figure 1.1 Conceptual diagram showing transmittance (T) versus intensity (I) of a saturable absorber (SA). Pulse shaping by the SA is illustrated.

Passive modelocking has allowed for pulse durations as short as 5 femtoseconds [2]. Passively modelocked lasers have had enormous and widespread scientific impact. The 1999 Nobel Prize in Chemistry was awarded for using femtosecond spectroscopy to study transition states in chemical reactions. The 2005 Nobel Prize in Physics was awarded in part for the development of the optical frequency comb technique.

In 1990, the discovery of Kerr-lens modelocking in a titanium-doped sapphire laser (Ti:sapphire) revolutionized the field of short-pulse generation [3]. Kerr-lens modelocking uses self-focusing inside the gain crystal to produce an intensity dependent loss through cavity misalignment. Properties of the Ti:sapphire crystal such as a large gain spectrum (from 650 – 1100 nm) and high thermal conductivity allow the laser to be a versatile source of ultrafast pulses. Largely due to the success of Ti:sapphire lasers, there has been an explosion in demand for femtosecond sources for applications outside the research laboratory. The large spectral bandwidth, short pulse duration, and

high peak power achievable with Ti:sapphire lasers have found uses in the telecommunications and biomedical industries to name a few.

While solid-state lasers such as Ti:sapphire typically provide the best performance, they lack long-term stability outside a laboratory environment. Moreover, they are not easily integrated devices. These lasers tend to occupy a large footprint (~ 1 m^2), require 10-kW or more of electrical power, and need several gallons per minute of cooling water for operation. Consequently, solid-state lasers lack practicality outside the laboratory, and they typically require a laser expert for long-term operation.

Modelocked fiber lasers are rapidly becoming viable alternatives to solid-state devices. Fiber lasers offer greater stability, compact design (a footprint of ~ 0.05 m^2 which can literally fit in the palm of a hand), and reduced alignment sensitivity. Furthermore, they provide excellent beam quality, as they operate at the fundamental transverse fiber mode. Optical fiber possesses a large ratio of surface area to volume, which allows for outstanding heat dissipation and precludes the need for water cooling. A simple conception of a femtosecond fiber laser is a loop of single-mode fiber (SMF), where a portion of the fiber is doped with a rare earth element for gain. An SA is used to modelock, and output is taken from a fiber-spliced coupler. A fiber-coupled laser diode is used as a pump source. This basic design is shown in Figure 1.2 below.

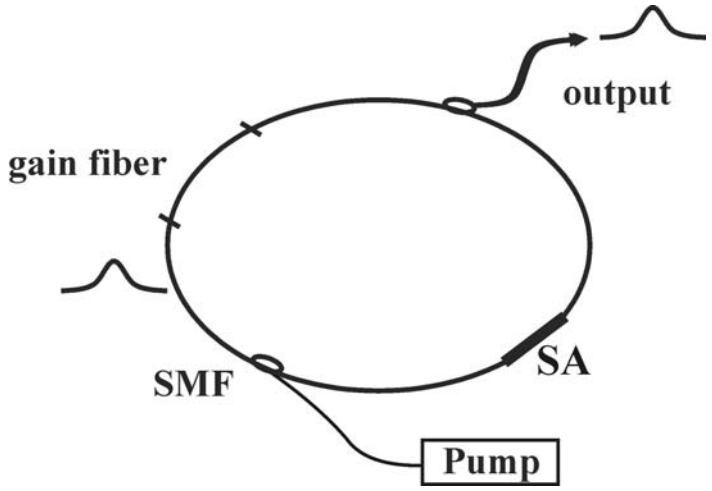

Figure 1.2 Basic design for one type of modelocked fiber laser. SMF: single-mode fiber, SA: saturable absorber.

The main drawbacks of fiber lasers include a smaller range of tunability and a tendency to produce much lower pulse energies, longer pulse durations, and lower pulse quality compared to solid-state lasers. Despite limited tunability, SMF can be doped with different rare-earth ions to lase at very important wavelengths, including 1.55 μm for telecommunications and 1.0 μm for biomedical applications. Fiber lasers have historically produced less energetic, longer, and lower-quality pulses mainly due to excessive fiber nonlinearites. Because light is guided inside a fiber core (diameter ~ 10 μm), fiber nonlinearites are enhanced by about four orders of magnitude over a typical open-air laser beam propagating through bulk material. Excessive nonlinear phase accumulation tends to destroy single-pulse operation. This thesis focuses on improving pulse energy and pulse duration from femtosecond fiber lasers by overcoming limitiations imposed by fiber nonlinearities.

1.2 Pulse formation and propagation in fiber lasers

Femtosecond pulse formation in a fiber laser is dominated by an interplay between group-velocity dispersion (GVD), the Kerr nonlinearity of the fiber through self-phase modulation (SPM), and amplitude modulation due to the SA. Under extreme conditions, higher-order dispersive and nonlinear effects become important. Typical higher-order effects include third-order dispersion (TOD) and Raman gain. Other effects which are generally weaker include pulse shaping due to gain dispersion and bandwidth limitations of the fiber components.

The governing equation of motion for pulse propagation is referred to as the nonlinear Schrodinger equation. In its simplest form, it is given by:

$$\frac{\partial A}{\partial z} = i\gamma|A|^2 A - i\frac{1}{2}\beta_2 \frac{d^2 A}{\partial t^2} \quad (1.1)$$

Here, A is the amplitude of the pulse envelope. The parameter β_2 is the GVD parameter which is the coefficient of the second-order term in the expansion of the wave number about the center frequency. The parameter γ is the nonlinear coefficient which is proportional to the nonlinear index of refraction, n_2. Equation (1.1) assumes an instantaneous nonlinear response, which is valid for pulse durations > 1 ps. For femtosecond pulses, the effects of molecular contributions to the fiber nonlinearities must be included (The Raman response must the included). Also, for pulse durations shorter than ~ 50 fs, TOD must be included.

Solutions to Equation (1.1) depend on the relative strengths and signs of the dispersive and nonlinear terms. An interesting and very practical case occurs under the conditions of anomalous dispersion and positive (self-focusing) nonlinearity. In this case, the resulting pulse has a hyperbolic-secant intensity profile. The linear and nonlinear contributions to phase exactly cancel, and the pulse propagates undistorted. Such a solution is called a soliton. Soliton propagation in optical fiber was first predicted by Hasegawa *et. al* [4].

1.3 Numerically modeling pulse propagation in fiber lasers

Ultrafast fiber oscillators are complex devices from the standpoint of understanding the underlying physical processes. A pulse propagating in a fiber laser undergoes dispersive and nonlinear interactions, as well as amplitude and frequency modulation. Moreover, all of these processes occur in the presence of feedback. As a result, there is currently no analytic theory describing modelocked fiber lasers, and intuition is gained from numerically solving a modified version of Equation (1.1). Accounting for gain, loss, and amplitude modulation due to the SA, the governing equation is referred to as the Ginzburg-Landau equation, which is given below.

$$\frac{\partial A}{\partial z} = i\gamma|A|^2 A - i\frac{1}{2}\beta_2\frac{d^2A}{\partial t^2} + (g-l)A - g''\frac{\partial^2 A}{\partial t^2} - q|A|^2 A \quad (1.2)$$

The third term on the right of Equation (1.2) includes gain and loss; the fourth term describes gain dispersion, and the last term describes self-amplitude modulation of the SA.

Using split-step Fourier techniques, Equation (1.2) can be numerically solved. Starting from noise, pulsed solutions are found. Figure 1.3 displays a typical result.

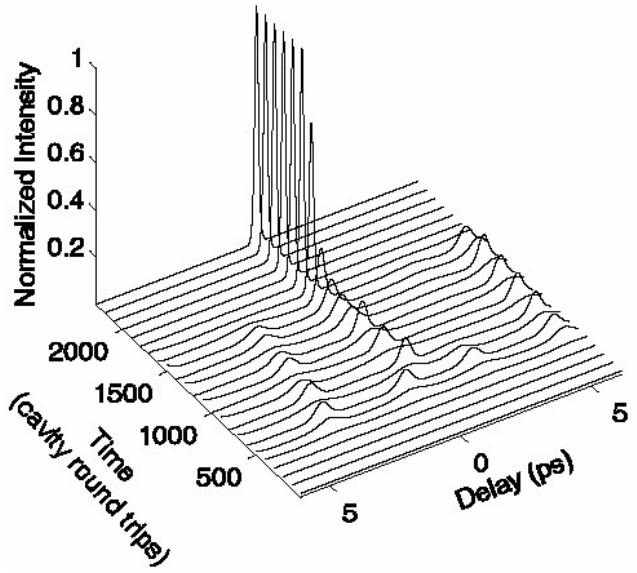

Figure 1.3 Simulation showing the buildup of a modelocked pulse from noise.

1.4 The role of the saturable absorber in fiber lasers

An ideal SA has very deep modulation, meaning the difference between the transmission of high and low intensities is large. Also, an ideal SA has an instantaneous response time, which allows for the generation of very short (i.e. femtosecond) pulses. The SA helps to initiate modelocking by shaping a pulse from noise. When the pulse duration reaches the picosecond regime, effects due to GVD and SPM take over and further shape the pulse to femtosecond durations. At this point, the SA serves to stabilize modelocked operation against the buildup of noise by continually cleaning up the pulse every round trip.

A real SA is based on saturation of a resonant transition, usually between the energy bands of a semiconductor. Real SA's typically have response times on the order of picoseconds. An artificial saturable absorber (ASA) utilizes a nonlinear phase shift between two interfering signals. When the linear phase bias is properly set, the ASA provides constructive interference for higher intensities and destructive interference for lower intensities. Thus, higher intensities are preferentially transmitted, and a pulse can be shaped from noise. Passively modelocking a laser through the coherent addition of two signals is referred to as additive-pulse modelocking (APM). The first demonstration of APM in a laser was performed by Mollenauer *et. al* [5].

The main advantage of using APM is that the corresponding ASA has a virtually instantaneous response time. The main disadvantage is that it relies on the interference of two signals, making the response periodic with pulse energy. Consequently, for a given linear phase bias, very high pulse energies can "overdrive" the ASA. This results in decreasing transmission for higher intensities, which works against pulse formation. Overdriving the ASA is shown schematically in Figure 1.4.

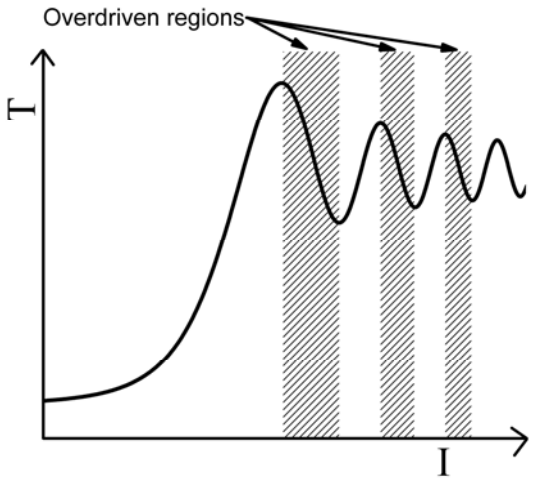

Figure 1.4 Conceptual diagram of an artificial saturable absorber. The transmittance (T) versus intensity (I) is cyclical in nature, with the overdriven regions indicated.

Most of the fiber lasers reported in this thesis use nonlinear polarization evolution (NPE) as an ASA for starting and stabilizing modelocked operation [6]. It is well known that the Kerr effect due to the self-focusing nonlinearity of a material rotates the orientation of elliptically polarized light. The magnitude of rotation per unit distance is proportional to the intensity of light. Figure 1.5 is a schematic of a typical setup for generating NPE in a fiber laser. The arrows in the figure represent linearly polarized light at small and large intensity, respectively. Likewise, the ellipses represent elliptically polarized light.

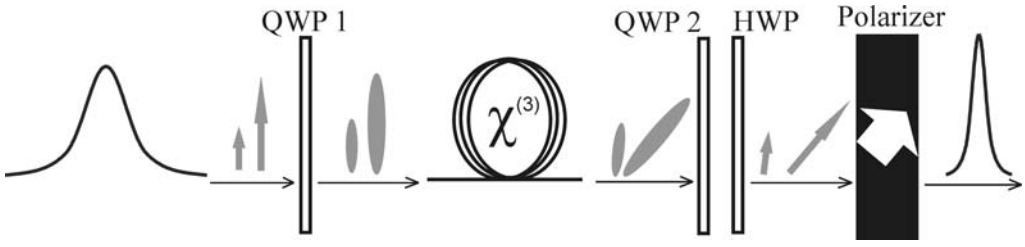

Figure 1.5 Schematic showing NPE action on a pulse. QWP1: first quarter wave plate, QWP2: second quarter wave plate, HWP: half wave plate, $\chi^{(3)}$: third-order Kerr nonlinearity of optical fiber.

The first quarter wave plate shown in Figure 1.5 is used to convert the polarization state from linear to elliptical before the light enters the Kerr medium (the SMF). The second quarter wave plate converts the polarization back to linear. A half-wave plate is used to adjust the orientation of the linearly polarized light as it enters a polarizer. By properly biasing the wave plates, the polarizer preferentially transmits higher intensities, thus creating an ASA. Nonlinear polarization evolution is a form of APM in which the two signals represent the left- and right-circularly-polarized eigenstates of the light.

1.5 Soliton fiber lasers

Modelocked fiber lasers can be categorized according to the pulse evolution inside the laser cavity. Historically, the first fiber lasers were soliton-based lasers at 1.55 μm wavelength. In this type of laser, the fiber segment combines anomalous GVD with positive nonlinearity. The resulting solutions are soliton pulses which propagate with negligible change per round trip. The frequency sweep, or chirp, across the pulse is constant. Figure 1.6 illustrates this form of evolution in a laser cavity. To better illustrate the essential pulse propagation in Figure 1.6, the effects of gain, loss, and the SA on the pulse are not shown.

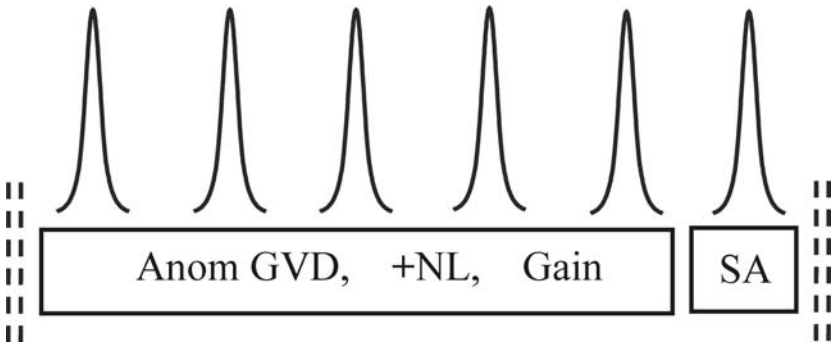

Figure 1.6 Cartoon showing the basic elements of a soliton fiber laser. The intra-cavity pulse evolution is shown.

Strictly speaking, a fiber laser cannot produce a perfect solition as there are perturbations to the pulse due to gain and loss. These perturbations cause the soliton to bleed energy in the form of dispersive waves. At specific frequencies, these dispersive waves resonate in the laser cavity and manifest themselves as spectral side bands. An example of this is shown in Figure 1.7.

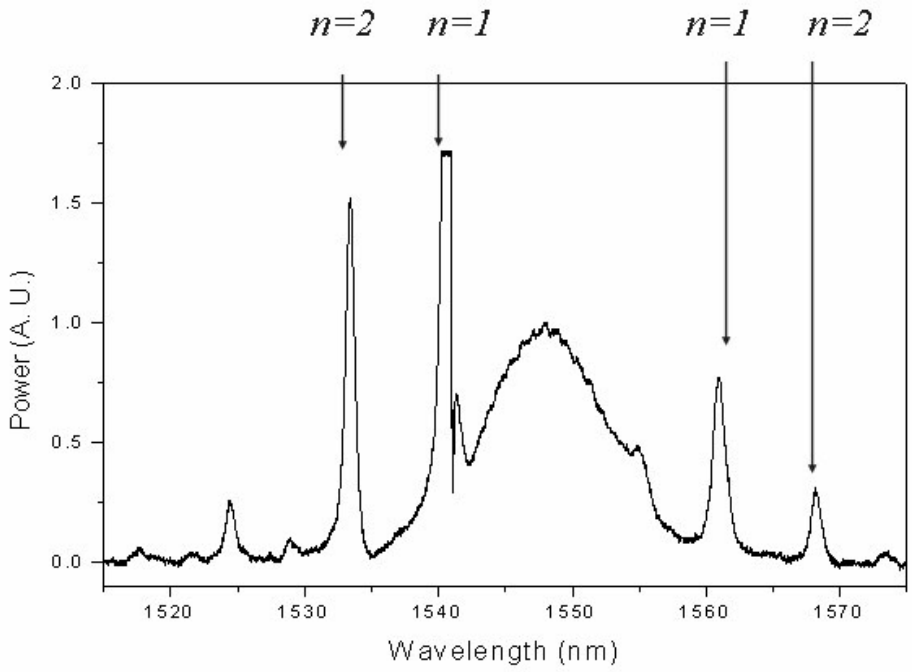

Figure 1.7 An example of spectral sidebands from a typical spectrum out of a modelocked Er-doped fiber laser. The order of the sideband is indicated by n.

The sidebands limit the spectral width of the pulse, which in turn constrains the pulse duration. The soliton energy and pulse duration are inversely related through the soliton area theorem by:

$$P_0 T_0^2 = \frac{|\beta_2|}{\gamma} \quad (1.3)$$

Where P_0 is the peak power and T_0 is the 1/e intensity duration. Consequently, spectral sideband generation ultimately limits the pulse energy. A more fundamental limitation to energy occurs when the accumulated nonlinear phase is too large to be balanced by the given pulse dispersion. This leads to optical wave breaking, shown in simulation in Figure 1.8. Wave breaking creates a severe practical limitation to soliton fiber lasers, resulting in pulse energies

around 0.1 nJ. In contrast, a Ti:sapphire laser can produce femtosecond pulses with 10- to 20-nJ energies.

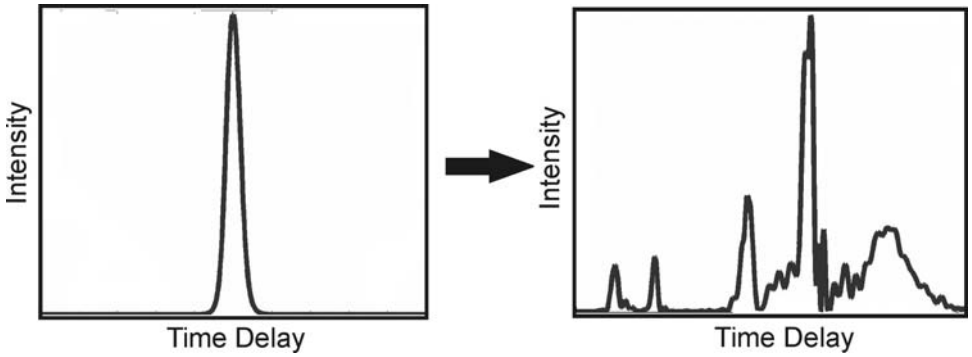

Figure 1.8 Illustration of a pulse undergoing optical wave breaking.

1.6 Higher pulse energy by avoiding excessive nonlinearities

One approach to avoiding excessive nonlinear phase shift is to increase the mode area of the optical fiber. Such large-mode-area fibers (LMA) exist, and they have been used with moderate success in fiber lasers[7,8]. The problem with this approach is that it results in a trade-off in numerical aperture (NA) in order the maintain single-mode operation. Reducing the NA results in larger bending losses. Also, using LMA fiber reduces the strength of NPE action, which makes pulsed operation harder to self-start.

Another approach is to amplify the output of a low energy fiber laser. Figure 1.9 shows an example of a master-oscillator-power-amplifier (MOPA) setup for an Yb fiber laser.

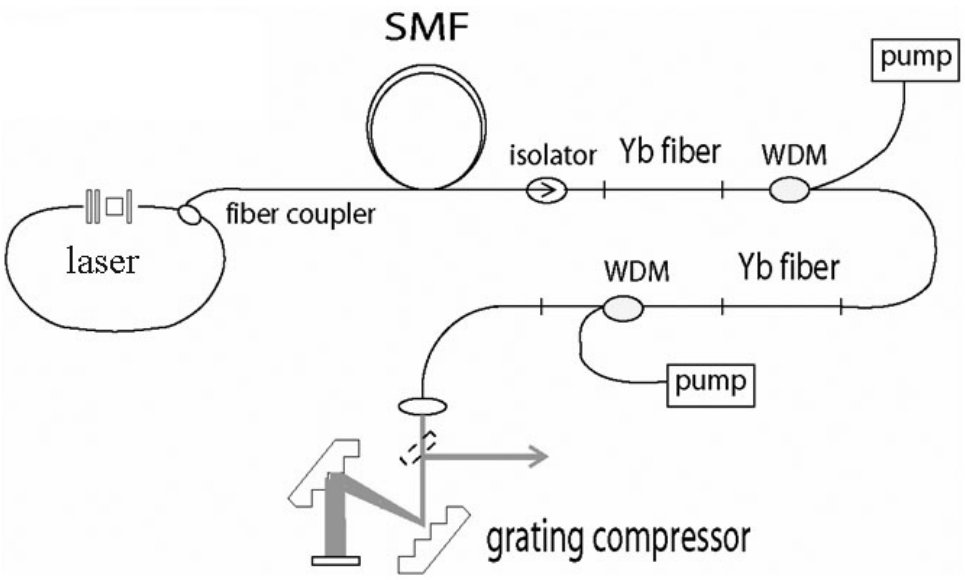

Figure 1.9 A Yb fiber laser coupled to a two-stage fiber amplifier. SMF: single-mode fiber, WDM: wavelength-division-multiplexing coupler.

This technique is quite successful. A stretched-pulse Yb fiber MOPA based on the design shown in Figure 1.9 has produced 8-nJ pulses [9]. A deficiency of amplified fiber systems is that they have added complexity (and cost). Another problem is avoiding the buildup of noise in the amplified output. For these reasons, this thesis focuses on generating high energies directly from fiber oscillators by exploiting nonlinearities through novel pulse evolutions.

1.7 Stretched-pulse fiber lasers

An effective way to control nonlinearity is to make the fiber laser with alternating segments of anomalous and normal GVD. The resulting pulse evolution breathes (stretches and compresses) during one round trip.

Figure 1.10 illustrates this type of pulse propagation, which is known as stretched-pulse evolution [10]. Stretched-pulse evolution in a fiber laser is analogous to dispersion-managed solitons in telecommunications systems [11].

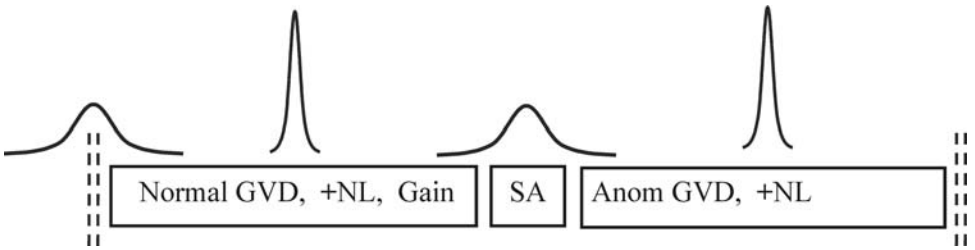

Figure 1.10 Cartoon showing the basic elements of a stretched-pulse fiber laser. The intra-cavity pulse evolution is shown.

The stretched-pulse experiences two minima durations per round trip. The chirp across the pulse changes sign twice per round trip. Because the chirp varies throughout the laser cavity, the output pulse usually has to be dechirped, unlike a soliton fiber laser. Figure 1.11 is a typical stretched-pulse spectrum.

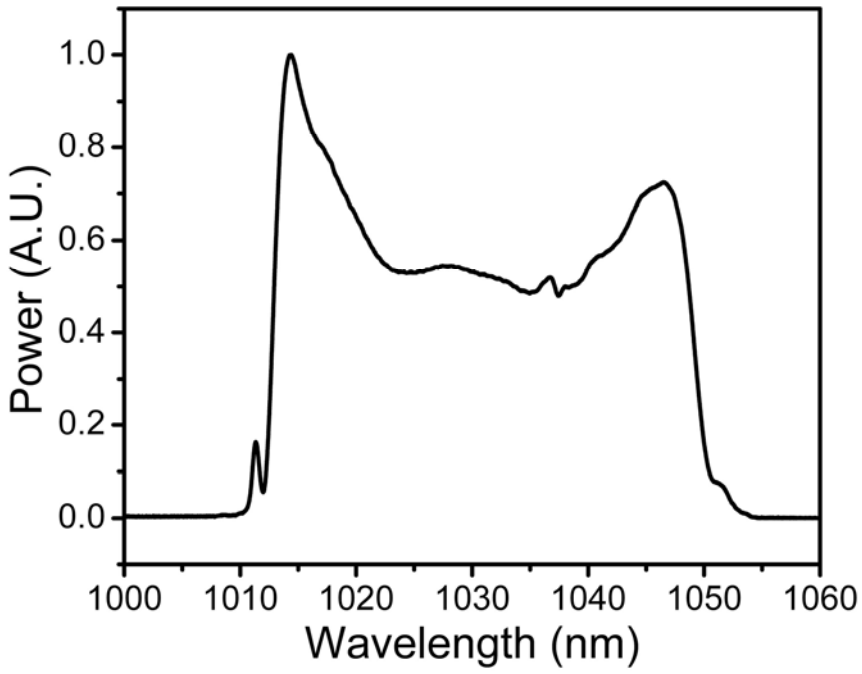

Figure 1.11 A typical stretched-pulse spectrum from a Yb-doped fiber laser.

It is important to note the lack of spectral sidebands in Figure 1.11. This is due to the fact that the pulse breathes inside the laser, which disrupts the phase-matching to dispersive waves. This is a beneficial side effect of stretched-pulse evolution since the pulse does not bleed as much energy due to intra-cavity perturbations. Much of the structure at the spectral wings in Figure 1.11 comes from the SA, which rejects the low-intensity wings of the chirped pulse (effectively rejecting the spectral extremes). The spectrum circulating inside the laser cavity is cleaner. Even though the output spectrum is structured, the resulting intensity profile is roughly Gaussian, which is typical of stretched-pulse operation. Because the pulse duration breathes, nonlinear phase accumulation is decreased due to a longer average pulse duration. Stretched-pulse fiber lasers can produce pulse energies on the order of 1 nJ, with the highest published energy being ~ 3 nJ [12].

Stretched-pulse Er-doped fiber lasers which operate at 1.55 μm wavelength can be made entirely out of optical fiber. This is because standard SMF has anomalous GVD, and the Er-doped fiber usually has normal GVD. Fiber lasers that operate around 1.0 μm, such as Yb- and Nd-doped fiber lasers, typically need diffraction gratings or prisms to provide anomalous GVD. This is because the SMF has normal GVD at this wavelength. Recently however, Yb fiber lasers have been modelocked using photonic crystal fiber (PCF) [13] and photonic bandgap fiber (PBF) [14] to provide anomalous GVD.

1.8 Self-similar fiber lasers

More recently, Ilday *et. al.* demonstrated the self-similar evolution of pulses inside a fiber laser [15]. A self-similar pulse is a solution to the nonlinear Schrodinger equation having a parabolic intensity profile. The pulse evolves asymptotically as a scaled version of itself inside the normal GVD segment of the laser cavity. This is shown schematically in Figure 1.12.

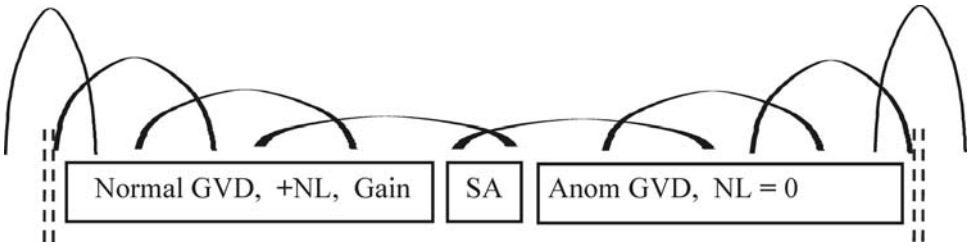

Figure 1.12 Cartoon showing the basic elements of a self-similar fiber laser. The intra-cavity pulse evolution is shown.

As in Figures 1.6 and 1.10, the effects of gain, loss, and the SA on the pulse are not shown in order to better illustrate the essential pulse evolution. It

should be noted that the self-similar laser has negligible nonlinearity in the anomalous dispersion segment. This is to avoid soliton pulse shaping, and it is achieved in practice by using diffraction gratings or prisms to create anomalous GVD. Inside the normal GVD segment, the combined effect of GVD and SPM results in the accumulation of a linear chirp across the pulse. This has been shown to make the pulse robust against optical wave breaking [16]. The pulse is always positively chirped inside the laser cavity; however, it can be dechirped external to the laser to transform limit. A typical self-similar spectrum is shown below in Figure 1.13. The key features are a roughly parabolic top and steep sides.

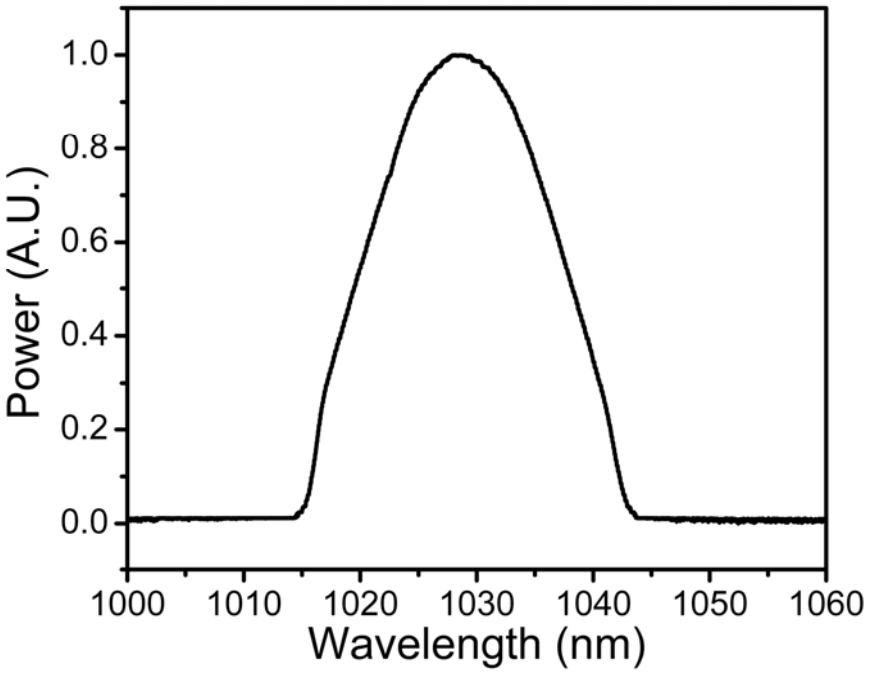

Figure 1.13 A typical self-similar spectrum from an Yb-doped fiber laser.

Numerical simulations of a self-similar Yb-doped fiber laser in Reference [15] indicate that 100-nJ pulse energies should be possible. In the

first attempts to generate these kinds of energies, which will be discussed in Chapter 2, there were indications that overdriving the ASA (not optical wave breaking) limited the pulse energy to ~ 10 nJ.

1.9 Wave-breaking-free fiber lasers

A fourth type of pulse evolution in fiber lasers has been observed in experiment, although not seen in simulation [17]. This has been referred to as wave-breaking-free evolution. The pulse is highly negatively chirped as it enters the normal GVD segment, and it decreases monotonically in duration throughout most of the segment, reaching a minimum duration near the end. The pulse evolution is qualitatively between stretched-pulse operation, where the pulse minima lie in the middle of the dispersion segments, and self-similar operation, where the single pulse minimum is at the beginning of the normal GVD segment. In many respects, wave-breaking-free evolution is like self-similar evolution running backwards. Figure 1.14 illustrates this in a laser.

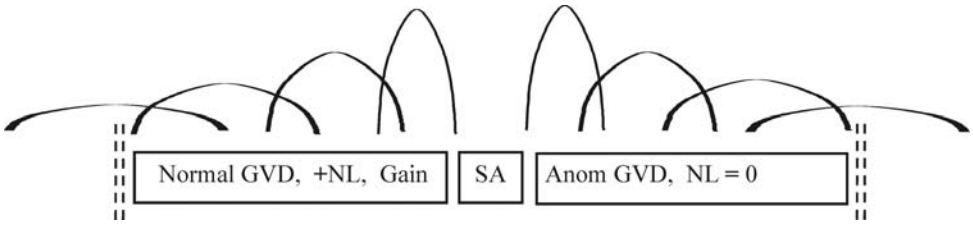

Figure 1.14 Cartoon showing the basic elements of a wave-breaking-free fiber laser. The intra-cavity pulse evolution is shown.

The pulse evolution shown in Figure 1.14 is an idealization of what is actually observed. Based on experiments with a Yb fiber laser, some of which will be discussed in this thesis, it is believed that the pulse actually experiences two

minima durations very close to each other – one near the end of the normal GVD segment, and the other near the beginning of the anomalous GVD segment. This "kink" in the evolution is not shown in Figure 1.14 to emphasize the essential elements of the pulse evolution. Also, as before, the effects of gain, loss, and the SA on the pulse are not shown. A characteristic wave-breaking-free spectrum is shown in Figure 1.15.

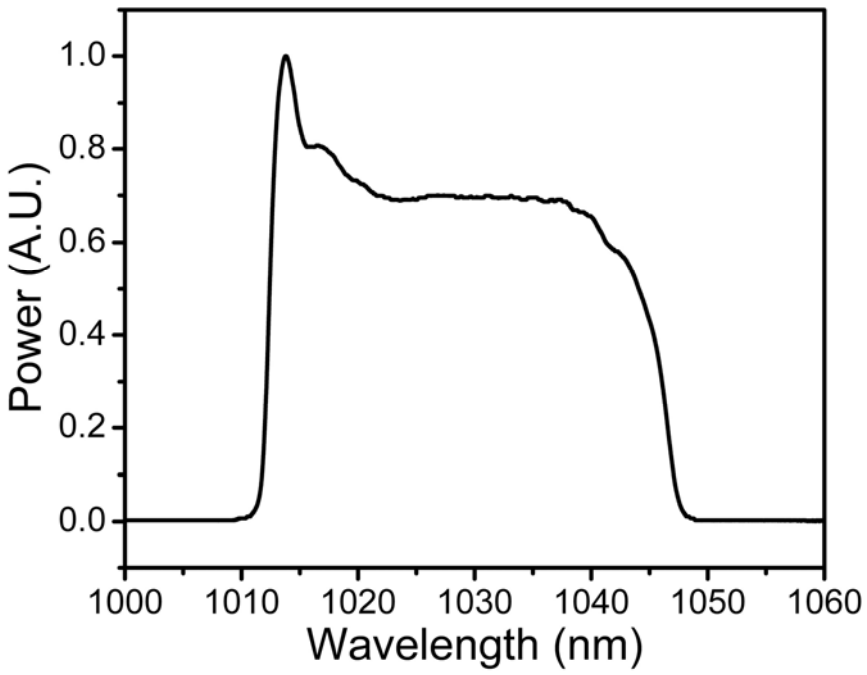

Figure 1.15 A typical wave-breaking-free spectrum from an Yb-doped fiber laser.

Due to the lack of an analytic theory and the fact that this mode is not seen in simulation, understanding of wave-breaking-free pulse evolution is in its infancy. For example, the effects of having appreciable nonlinear phase in the anomalous dispersion segment are not known. Experimentally, the pulse energy of a wave-breaking-free laser can approach ~10-nJ as in self-similar lasers, making this mode of evolution very attractive for applications.

1.10 Preface to thesis

Chapters 2 and 3 of this thesis focus on self-similar evolution as a route to achieving high-energy femtosecond pulses from a fiber laser. Limitations to pulse energy are explored, and a new form of pulse evolution is reported, which is called chirped-pulse evolution. Chapter 4 describes a technique for generating very high peak powers (> 100 kW) from fiber lasers operating in the wave-breaking-free regime. Chapter 5 focuses on generating few-cycle pulses from fiber lasers, which is very challenging given the large nonlinear and dispersive phase accumulated in the SMF. Chapter 6 covers some experiments in which a semiconductor saturable absorber mirror (SESAM) is used to modelock a fiber laser. Finally, Chapter 7 briefly discusses current and future directions.

All of the work reported in this thesis focuses on Yb-doped fiber lasers which operate around 1-μm wavelength. This wavelength is very useful for applications in medicine and biology. The lasers reported here represent a major step toward producing solid-state performance from a fiber oscillator.

BIBLIOGRAPHY

[1] A.J.D. Maria, D.A. Stetser, and H. Heynau, "Self mode-locking of lasers with saturable absorbers," Appl. Phys. Lett. **8**, 174 (1966).

[2] U. Morgner, F. X. Krtner, S. H. Cho, Y. Chen, H. A. Haus, J. G. Fujimoto, E. P. Ippen, V. Scheuer, G. Angelow, T. Tschudi, "Sub-two-cycle pulsesfrom a Kerr-lens mode-locked Tisapphire laser," Opt. Lett **24,** 411 (1999).

[3] D. Spence, P. Kean, and W. Sibbett, "60-femtosecond pulse generation from a self mode-locked Ti:Sapphire laser," Opt. Lett. **16**, 42 (1991).

[4] A. Hasegawa and F. Tappert, "Transmission of stationary nonlinear optical pulses in dispersive dielectric fibers with anomalous dispersion," Appl. Phys. Lett. **23**, 142 (1973).

[5] L.N. Mollenauer and R.H. Stolen, "The soliton laser," Opt. Lett. **9**, 13 (1984).

[6] M. Hofer, M. E. Fermann, F. Harberl, M. H. Ober, and A. J. Schmidt, "Mode locking with cross-phase and self-phase modulation," Opt. Lett. **16**, 502 (1991).

[7] M.A. Arbore, M.M. Fejer, M.E. Fermann, A. Hariharan, A. Galvanauskas, and D. Harter, "Frequency doubling of femtosecond erbium-fiber soliton lasers in periodically poled lithium niobate," Opt. Lett. **22**, 13 (1997).

[8] N.G.R. Broderick, H.L. Offerhaus, D.J. Richardson, and R.A. Sammut, "Power Scaling in Passively Mode-Locked Large-Mode Area Fiber Lasers," IEEE Photon. Tech. Lett. **10**, 1718 (1998).

[9] F.Ö. Ilday, H. Lim, J.R. Buckley, and F.W. Wise, "Practical all-fiber source of high-power, 120-fs pulses at 1 μm," Opt. Lett. **28**, 1362 (2003).

[10] K. Tamura, J. Jacobson, H.A. Haus, E.P. Ippen, and J.G. Fujimoto, "77-fs pulse generation from a stretched-pulse mode-locked all-fiber ring laser," Opt. Lett. **18**, 1080 (1993).

[11] N.J. Smith, N.J. Doran, W. Forysiak, and F.M. Knox, "Soliton transmission using periodic dispersion compensation," J. Lightwave Technol. **15**, 1808 (1997).

[12] L.E. Nelson, S.B. Fleischer, G. Lenz, and E.P. Ippen, "Efficient frequency doubling of a femtosecond fiber laser," Opt. Lett. **21**, 1759 (1996).

[13] H. Lim, F.Ö. Ilday, and F.W. Wise, "Femtosecond ytterbium fiber laser with photonic crystal fiber for dispersion control," Opt. Expr. **10**, 1497 (2002).

[14] Lim, F.W. Wise, "Control of dispersion in a femtosecond ytterbium laser by use of hollow-core photonic bandgap fiber," Opt. Express **12**, 2231 (2004).

[15] F.Ö. Ilday, J.R. Buckley, W.G. Clark, F.W. Wise, "Self-Similar Evolution of Parabolic Pulses in a Laser," Phys. Rev. Lett. **92**, 3902 (2004).

[16] D. Anderson, M. Desaix, M. Karlsson, M. Lisak, and M.L. Quiroga-Teixeiro, "Wave-breaking-free pulses in nonlinear-optical fibers," J. Opt. Soc. Am. B **10**, 1185 (1993).

[17] F.Ö. Ilday, J.R. Buckley, H. Lim, F.W. Wise, and W.G. Clark, "Generation of 50-fs, 5-nJ pulses at 1.03 microns from a wave-breaking-free fiber laser," Opt. Lett **28**, 1365 (2003).

Chapter 2

Femtosecond Fiber Lasers with Pulse Energies Above 10 nJ *

2.1 Introduction

Femtosecond fiber lasers offer several advantages over bulk solid-state lasers, including greater stability, reduced alignment sensitivity, and compact design. Furthermore, fiber lasers are very efficient. These qualities make short-pulse fiber lasers attractive for use in applications. However, mode-locked fiber lasers have lagged behind solid-state lasers with regard to the pulse energy, which is limited by excessive nonlinear phase shifts accumulated on propagation through the fiber.

Femtosecond pulse formation in a fiber laser is dominated by the interplay between group-velocity dispersion (GVD) and the Kerr nonlinearity of the fiber. An effective saturable absorber is needed to start and stabilize the pulse train, and nonlinear polarization evolution (NPE) is commonly employed for this purpose [1].

* J.R. Buckley, F.Ö. Ilday, T. Sosnowski, and F.W.Wise, Opt. Lett. 30, 1888 (2005).

Fiber lasers can be constructed entirely from anomalous-GVD fiber to operate in the soliton regime, where the pulse energy is limited by the soliton area theorem to ~0.1 nJ. At higher energy, wave-breaking occurs and is manifested as multiple pulsing. Stretched-pulse lasers are constructed with fiber segments with normal and anomalous GVD [2] and have produced 100-fs pulses with energy as high as 2.7 Nj [3]. A laser based on double-clad Yb fiber produced 11.8-nJ chirped pulses (110 mW average power), which were dechirped to 200 fs outside of the laser [4]. Although the pulse energy from this laser is high, the use of double-clad fiber along with an acousto-optic modulator to assist mode-locking naturally counter some of the main benefits of fiber sources.

Theoretically, wave-breaking is suppressed if a pulse develops a monotonic frequency chirp as it propagates. Such a pulse evolves self-similarly; i.e., the pulse is always a scaled version of itself. These pulses tend toward a parabolic shape and accumulate a linear chirp. Ilday *et. al.* recently showed that self-similar propagation can occur in a laser oscillator [5]. This represents a new regime of operation of modelocked lasers. The evolution of the pulse as it traverses the laser is fundamentally distinct from the evolution in soliton and stretched-pulse lasers. The pulse is always positively chirped inside the laser, with the temporal duration varying from ~3 to ~50 times the transform limit. However, it can be dechirped outside the laser to the transform limit. According to numerical simulations, lasers based on self-similar evolution can generate stable pulses with energies two orders of magnitude larger than are possible by other means. In the initial experimental demonstration, the pulse energy was intentionally limited to 2 nJ to isolate the pulse evolution and avoid

the limitations of other processes in the laser (Reference [5]). A preliminary result of 10-nJ pulse energy was mentioned. Ilday *et. al.* also reported a Yb fiber laser that generated 5-nJ pulses as short as 50-fs by avoiding wave breaking, but the intracavity pulse evolution was not self-similar [6]. In this paper, the pulse evolution was referred to as wave-breaking-free. To our knowledge, this performance represents the highest peak power (85 kW) and average power (200 mW) produced by a femtosecond fiber laser to date.

Here we report an investigation of the maximum pulse energies and peak powers that can be obtained from a femtosecond fiber oscillator. Pulse energies as high as 14 nJ can be generated, and the pulses can be dechirped to ~100 fs duration. The results suggest that the pulse energy is limited by the use of NPE as the effective saturable absorber and not by optical wave breaking.

2.2 Experiment

We built a Yb fiber laser similar to those described in References [5] and [6] (Figure 2.1). Highly-doped (23,900 parts in 10^6) Yb gain fiber allows the use of a short (~60 cm) gain segment, which follows an ~4.65-m segment of single-mode fiber (SMF). Following the gain fiber, the pulse passes through 1.33 m of SMF. The pulse then travels through quarter- and half-wave plates for the NPE, and a pair of diffraction gratings that provide anomalous GVD before returning to the SMF. The laser is pumped in core by two fiber-coupled 500-mW diodes or by the polarization-combined outputs of two master-oscillator power-amplifiers. Approximately 800 mW of pump power at 980 nm could be coupled into the gain fiber, which produced a continuous-wave output

power of ~500 mW. The output is taken from the NPE rejection port. The pulse repetition rate was 28 MHz in the experiments reported here. The laser produces positively chirped pulses, which are dechirped with a grating pair external to the cavity.

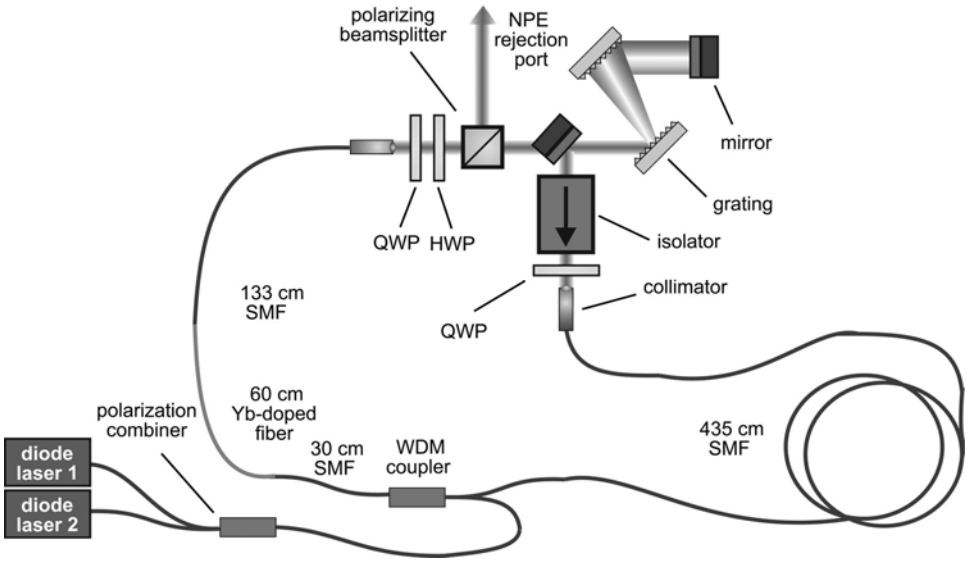

Figure 2.1 Schematic of fiber laser: HWP, half-wave plate; QWP, quarter-wave plate; WDM, wavelength division multiplexer.

A systematic search for the maximum pulse energy and peak power was undertaken. Theoretically, self-similar pulses with increasing energy can be tolerated with increasing normal cavity GVD (Reference [5]). Starting with the cavity GVD near zero, the wave plates (i.e., the NPE) are adjusted to produce a stable pulse train with maximum power. Once the maximum energy is obtained at a given value of the net GVD, the GVD is then increased slightly and the wave plates are readjusted to produce a stable pulse train. In each case, single-pulse operation is verified by monitoring the pulse train with a fast detector (~0.5-ns resolution) and a long-range (200 ps) autocorrelation. In addition, we monitor the spectrum with a high-resolution (0.07 nm) optical spectrum analyzer against the presence of secondary pulses.

Information about the intracavity pulse evolution is inferred from the magnitude of anomalous GVD required to dechirp the pulse. A stretched-pulse laser has minima of the pulse duration near the middle of each segment of the dispersion map. For average output powers above ~50 mW (which corresponds to nominal single-pulse energies ~2 nJ), stretched-pulse operation produces multipulsing. In contrast, the modes of operation that allow stable pulses with higher energies have minima of the pulse duration near either end of the SMF segment.

A convenient experimental signature of the self-similar regime is the characteristic spectral shape [(Figure 2.2(a)] with its approximately parabolic top and steep sides. In practice, the wave plates are adjusted to produce this spectrum. With a net GVD of 0.008 +/- 0.002 ps^2, ~5-ps pulses of 14-nJ energy were generated in self-similar operation. The corresponding average power was 400 mW.

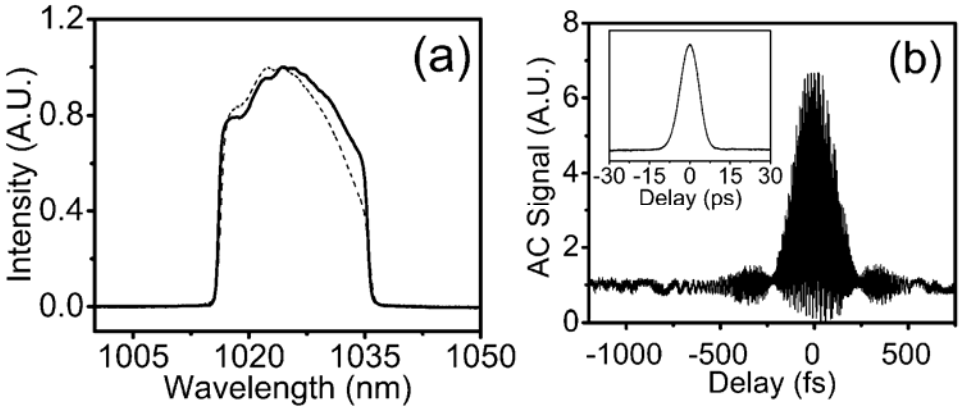

Figure 2.2 (a) Spectra of 14-nJ pulses transmitted (dotted curve) and rejected (solid curve) from the NPE port in self-similar operation. (b) Dechirped autocorrelation of pulses rejected from the NPE port. Inset, intensity autocorrelation of the chirped output pulse.

These pulses could be dechirped to 170 fs [Figure 2.2(b)], which exceeds the Fourier-transform limit by ~15%. The anomalous dispersion required to dechirp the output pulses is approximately 0.25 ps^2, whereas the intra-cavity grating pair provides 0.15 ps^2. Therefore, we conclude that the pulse duration is minimum (but not transform limited) near the beginning of the SMF. These observations are consistent with the evolution observed in numerical simulations (Reference [5]). The resemblance of the spectra transmitted and rejected by the NPE port [Figure 2.2(a)] suggests that NPE does not play a strong role in pulse shaping in this regime, as expected theoretically.[5] We found that a minimum of ~1 m of SMF is needed between the Yb gain fiber and the output collimator to obtain self-similar operation at 28 MHz. We suspect that the nonlinear phase shift in that segment enhances the NPE, which is otherwise rather weak owing to the large output coupling.

High-energy pulses are also produced by a mode of operation distinct from the self-similar propagation described above. Adjustment of the wave plates can produce the broader and more-structured spectrum of Figure 2.3(a).

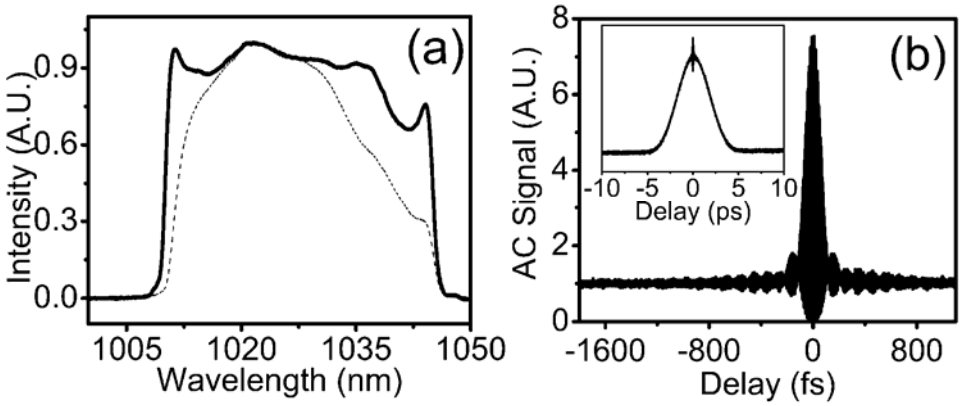

Figure 2.3 (a) Spectra of 13-nJ pulses transmitted (dotted curve) and rejected (solid curve) from the NPE port. (b) Dechirped autocorrelation of pulses rejected from the NPE port. Inset, intensity autocorrelation of the chirped output pulse.

In this case, the dispersion required to dechirp the output pulses is approximately 0.065 ps^2, whereas the intracavity dispersion remains at 0.15 ps^2. This implies that the pulse enters the SMF with a significant negative chirp, which would decrease in magnitude as the pulse approaches the gain fiber. We estimate that the pulse reaches minimum duration near the end of the SMF. Ilday *et. al.* obtained pulses with 85 kW peak power in a similar mode of operation which is referred to as wave-breaking-free (Reference [6]). This evolution is not exhibited by numerical simulations that model the NPE as a lumped element after the gain medium, so we do not understand it thoroughly. The difference between the spectra transmitted and rejected by the NPE port [Figure 2.3(a)] implies that the NPE plays a stronger role in the pulse shaping in this mode than in the self-similar mode. Pulse energies up to 13 nJ could be obtained. With a net cavity GVD of 0.004 +/- 0.002 ps^2, the chirped pulse duration was ~3 ps, and the dechirped pulse duration was 85 fs [Figure 2.3(b)], which is close to the transform-limited value obtained from the zero-phase

Fourier transform of the power spectrum. With new, high-efficiency gratings the dechirped pulse energy is 10 nJ and the peak power is 100 kW.

At lower repetition rates, higher pulse energies are energetically possible for a given average power, but we were unable to exceed the pulse energies above. For example, at 20 MHz, 10-nJ pulses were generated in self-similar operation, but only ~1 nJ could be obtained in the mode with pulse duration minimum near the gain fiber. At 15 MHz, only self-similar operation produced single-pulsing, and the pulse energy was ~4 nJ.

2.3 Analysis of Results

It is important to consider likely limitations to the pulse energy. The 13- and 14-nJ pulses were generated with all the available pump power. However, the proximity of multi-pulsing states and the relative difficulty to observe stable single-pulse trains convince us that the pulse energy has essentially reached the limits determined by nonlinearity. On the basis of the experiments reported here, we cannot decisively conclude whether the pulse energy is limited by wave breaking or by overdriving of the NPE (i.e., by the accumulation of such large phase shift that the transmission of the NPE is decreasing with intensity and thus works against pulse formation). However, numerical simulations that model the NPE as a lumped element, with transmittance increasing monotonically with pulse energy, predict that stable pulses should exist at energies exceeding 100 nJ (Reference [5]). This suggests that NPE is the current limitation. The experimental results support this suggestion to some extent. First, the highest pulse energies were obtained with the sacrifice of

self-starting operation. The largest energies may be accommodated by biasing the NPE such that the transmittance does not increase adequately at low energy. Second, the maximum single-pulse energy that can be achieved declines when the cavity length becomes comparable to the beat length of the fiber (5-10 m), which suggests that uncontrolled birefringence may be playing a role. Finally, the observation of a small amount of excess bandwidth in the highest-energy self-similar pulses suggests that small deviations from a linear chirp can be tolerated in propagation. Further work is clearly needed to understand the limitations to pulse energy. Simulations that model the NPE as distributed along the fiber should help identify the limitation to pulse energy and understand the mode of pulse propagation that has minimum pulse duration near the gain fiber.

Owing to the proximity of multi-pulsing states, careful alignment of the waveplates is required to obtain the maximum pulse energies, and mode-locking can be extinguished by environmental perturbations. On the other hand, with pulse energies in the range of 5-7 nJ, operation is stable indefinitely. The ~400-mW average powers are the highest obtained from a short-pulse fiber laser. This laser achieves greater than 50% optical efficiency when modelocked. Advances in pump diodes and the use of photonic-bandgap fiber for dispersion control [7] should allow the development of stable, integrated versions of the present laser.

2.4 Conclusion and Acknowledgements

In conclusion, we have experimentally demonstrated that a fiber laser can generate ~100-fs pulses with pulse energy greater than 10 nJ. Numerical simulations and preliminary observations suggest that NPE limits the pulse energy, and work is in progress to understand and circumvent this limitation.

Portions of this work were supported by the NIH, and NSF-ECS and Clark/MXR, Inc. The work in this chapter was performed with Ömer Ilday and Tom Sosnowski. The author thanks M. Mosley for assistance in taking measurements. The author acknowledges the support of the National Physical Science Consortium through a graduate research fellowship.

BIBLIOGRAPHY

[1] M. Hofer, M. E. Fermann, F. Harberl, M. H. Ober, and A. J. Schmidt, "Mode locking with cross-phase and self-phase modulation," Opt. Lett. **16**, 502 (1991).

[2] K. Tamura, J. Jacobson, H.A. Haus, E.P. Ippen, and J.G. Fujimoto, "77-fs pulse generation from a stretched-pulse mode-locked all-fiber ring laser," Opt. Lett. **18**, 1080 (1993).

[3] L.E. Nelson, S.B. Fleischer, G. Lenz, and E.P. Ippen, "Efficient frequency doubling of a femtosecond fiber laser," Opt. Lett. **21**, 1759 (1996).

[4] A. Albert, V. Coudec, L. Lefort, A. Barthelemy, "High-energy femtosecond pulses from an ytterbium-doped fiber laser with a new cavity design," IEEE Photon. Technol. Lett. **16**, 416 (2004).

[5] F.Ö. Ilday, J.R. Buckley, W.G. Clark, F.W. Wise, "Self-Similar Evolution of Parabolic Pulses in a Laser," Phys. Rev. Lett. **92**, 3902 (2004).

[6] F.Ö. Ilday, J.R. Buckley, H. Lim, F.W. Wise, and W.G. Clark, "Generation of 50-fs, 5-nJ pulses at 1.03 microns from a wave-breaking-free fiber laser," Opt. Lett **28**, 1365 (2003).

[7] H. Lim, F.W. Wise, "Control of dispersion in a femtosecond ytterbium laser by use of hollow-core photonic bandgap fiber," Opt. Express **12**, 2231-2235 (2004).

Chapter 3

Chirped-pulse fiber oscillator

3.1 Introduction

In the last chapter, it was seen that high-energy pulses could be generated in an ytterbium fiber laser operating in the self-similar regime. Self-similar pulse evolution requires normal group-velocity dispersion (GVD) to balance self-phase modulation (SPM) effects in the cavity [1]. Simulations predict rapidly increasing pulse energy with increasing cavity GVD [2]; however, the experiments in Chapter 2 indicate a maximum of 14-nJ is reached at a net GVD of roughly 0.008 ps^2. Overdriving the NPE is attributed with preventing higher energies.

The scaling of pulse energy with cavity GVD is not exclusively a property of self-similar operation. The same trend is seen in our experiments for stretched-pulse and wave-breaking-free evolution. Also, it is well-known that the highest pulse energies produced from solid-state lasers occur at net normal GVD. As the GVD becomes increasingly normal, the pulse duration tends to broaden with increasing energy, stabilizing it against wave breaking effects [3,4]. This observation was first made with a Ti:sapphire laser by Proctor *et. al.* [5]. Dudley *et. al.* later used frequency-resolved optical gating (FROG) to completely characterize a Ti:sapphire laser operating in this regime [6].

In this chapter, we investigate a Yb fiber laser under the condition of large normal GVD, where the highest attainable pulse energies are expected to occur. For fixed pulse energy, when the net GVD is increased above approximately 0.015 +/- 0.002 ps^2, the laser prefers to operate in a mode where the intra-cavity breathing is minimized (where the ratio of the longest to shortest pulse durations inside the cavity is approximately one). Experimental data is compared to numerical simulation, and these nearly static, highly chirped pulses are shown to be a limiting case of self-similar evolution at large normal cavity GVD. The data is also examined with respect to the analytic theory for additive-pulse modelocking (APM), which is valid for lasers in which the pulse changes per round trip are negligible [7,8].

3.2 Experiment

Figure 3.1 depicts the basic Yb fiber laser setup, which is almost identical to the setup in Chapter 2. Modelocking is initiated and stabilized through nonlinear polarization evolution (NPE) [9]. The laser repetition rate is approximately 30 MHz. For all modelocked states, the laser produces positively-chirped pulses, which are dechirped with a grating pair external to the cavity.

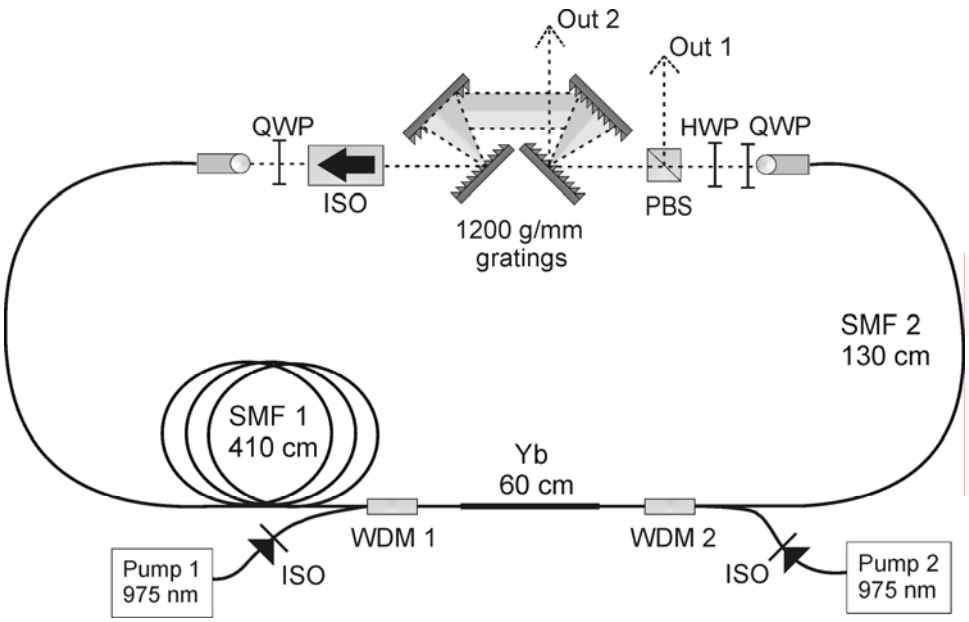

Figure 3.1 Yb fiber laser setup. SMF = single-mode fiber, QWP = quarter wave plate, HWP = half wave plate, PBS = polarizing beam splitter (NPE rejection port), ISO = isolator, WDM = fiber pigtailed couplers.

When the net GVD is less than ~0.010 +/- 0.002 ps^2, three distinct modes of pulse evolution are observed: stretched-pulse (in which the pulse breathes and experiences two minima durations per round trip) [10], self-similar, and another mode which qualitatively lies between stretched-pulse and self-similar. In the first demonstration of this other mode of evolution, it was referred to as wave-breaking-free [11]. As the net GVD is increased beyond ~0.010 +/- 0.002 ps^2, the laser prefers to operate in the self-similar or wave-breaking-free regimes. Beyond ~0.015 +/- 0.002 ps^2, the pulses become highly chirped with little intra-cavity breathing.

Beginning with self-similar operation near zero GVD, we incrementally increase the net GVD by reducing the separation between the intra-cavity gratings. At each step, the laser is modelocked and the NPE is biased (by

turning the waveplates) to find solutions with the highest pulse energy. Single-pulsing is verified down to 0.5 ns with a fast photodiode and out to ~ 100 ps with an interferometric autocorrelation measurement. The laser depicted in Figure 3.1 can not achieve stable modelocking when the GVD is increased beyond 0.044 +/- 0.002 ps^2. This is believed to be caused by inadequate NPE action at this large normal GVD. Some experimental evidence supports this claim. For example, by reversing the direction of the cavity, the laser can be modelocked out to 0.100 +/- 0.002 ps^2. Reversing the direction effectively increases the length of SMF after the Yb gain. This increases self-phase modulation (SPM), resulting in stronger NPE action. The laser cavity is arguably changed when operating in the reverse direction. Data taken at GVD values beyond 0.044 +/- 0.002 ps^2 is not presented here to preserve consistency, although it qualitatively fits the trends discussed below.

Figure 3.2 shows the progression of modelocked spectra with increasing GVD for a fixed pulse energy of ~ 7 nJ. Figure 3.2(a) corresponds to self-similar pulse evolution, as verified by measuring the pulse duration and chirp at the NPE port. The intra-cavity breathing ratio is approximately 9. Figures 3.2(b)-(e) correspond to highly chirped pulses with almost static breathing. The dechirped and chirped interferometric autocorrelation (AC) measurements corresponding to Figure 3.2(c) are also shown on the right. These AC measurements are typical of the highly chirped pulses represented by the modelocked spectra in Figures 3.2(a)-(e).

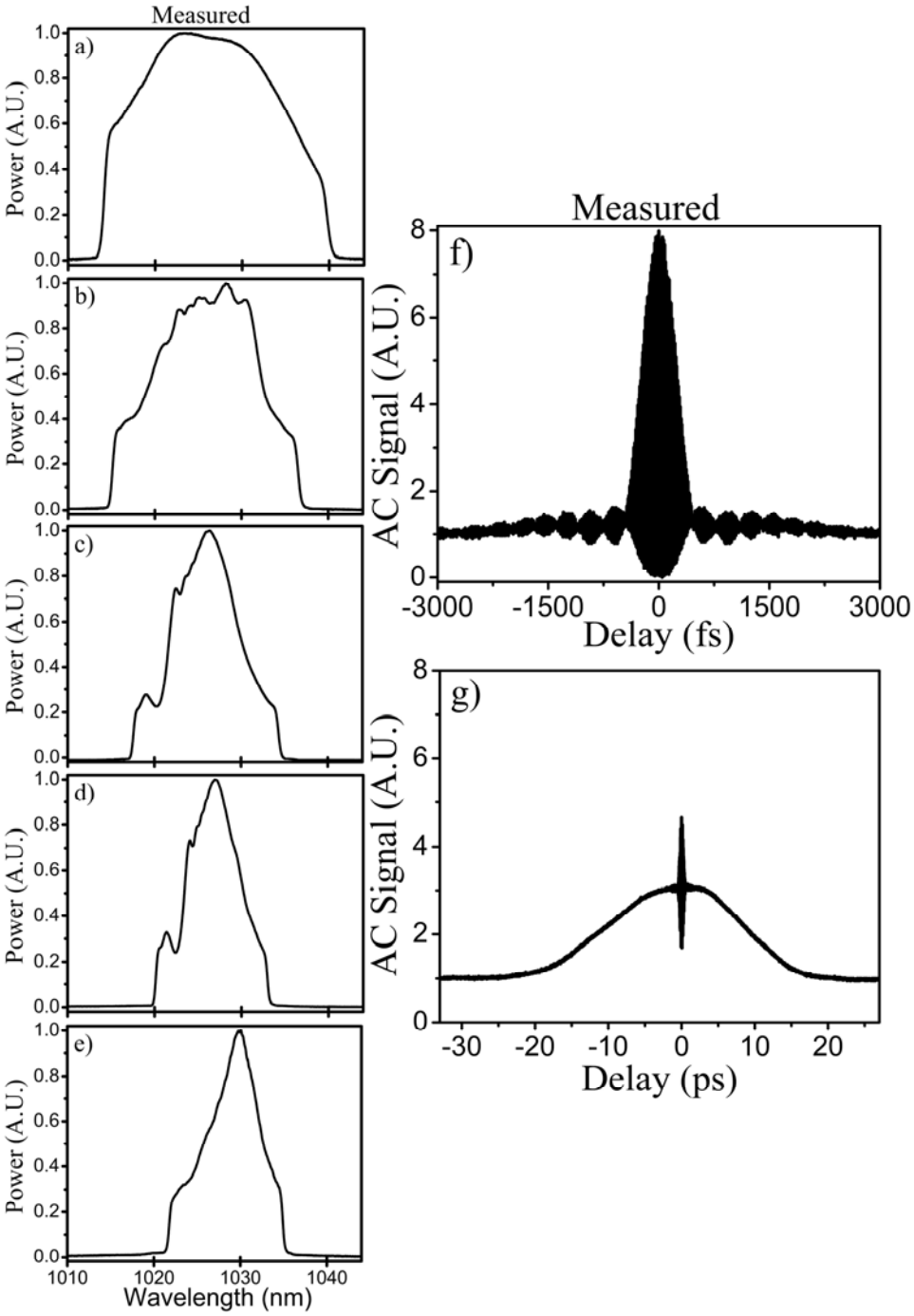

Figure 3.2 (left)measured modelocked spectra for 7-nJ pulses at different cavity GVD; (a) 0 ps^2, (b) 0.015 ps^2, (c) 0.028 ps^2 (d) 0.036 ps^2, (e) 0.043 ps^2 (right) (f) de-chirped autocorrelation and (g) chirped autocorrelations corresponding to spectrum (c).

The chirped-pulse AC has a full-width-at-half-maximum (FWHM) duration of ~20 ps, corresponding to a 14-ps chirped pulse. The dechirped pulse duration is estimated to be 180 fs, accounting for third-order-dispersion (TOD) added by the dechirp gratings. Although the dechirped AC shows some energy extending beyond 2 ps, long-range measurements confirm the lack of a large pedestal. There is an estimated 25% uncertainty in the measured chirped AC shown in Figure 3.2(g) owing to the fact that the pulse extends beyond the linear range of the autocorrelation measurement. An autocorrelator with larger dynamic range is necessary for more accurate measurements. As a result, the chirped-pulse durations quoted in this chapter are inferred by numerically adding the known phase of the dechirp gratings to the measured dechirped pulses. This technique works very well (to within a few percent) when we compare it to reliable chirped-pulse AC measurements, giving us confidence in our measurements.

Figure 3.3 shows a typical result of simulation for 1-nJ self-similar pulses. The simulated spectra are less structured than what is measured in Figure 3.2. Also, simulation predicts somewhat narrower spectral bandwidths; however, this likely due to the lower pulse energy. The trend of decreasing spectral width with increasing normal GVD is clearly seen in simulation.

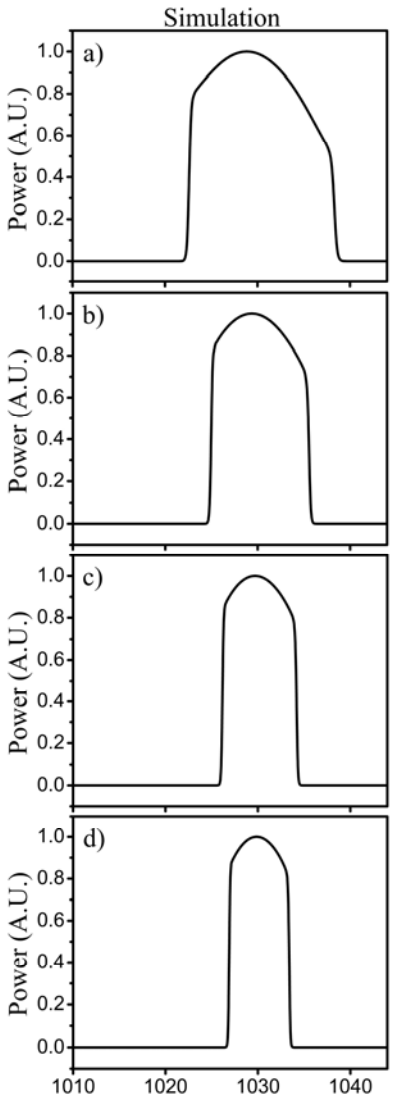

Figure 3.3: Simulated self-similar spectra for 1-nJ pulses at different cavity GVD; (a) 0.015 ps^2 (b) 0.025 ps^2, (c) 0.035 ps^2, (d) 0.045 ps^2

3.3 Comparison to self-similar operation

The highly chirped, nearly static pulse evolution observed at large normal GVD qualitatively resembles self-similar operation. The pulse is always positively chirped inside the laser cavity (unlike stretched-pulse or wave-breaking-free evolution). Also, the maximum pulse energy is measured to be ~10-nJ (unlike stretched-pulse operation which is limited to ~ 3-nJ femtosecond pulses due to optical wave breaking). Therefore, we are motivated to investigate how these highly chirped modes are related to self-similar operation.

Simulations of a self-similar Yb fiber laser (Reference [2]) predict that pulse energy increases exponentially with increasing normal GVD. Also, for fixed pulse energy, as the net GVD becomes increasingly normal, the self-similar pulses are expected to become long and highly chirped, resulting in a rapidly decreasing intra-cavity breathing ratio. Figure 3.4 shows the measured 7-nJ data along with the simulated trends.

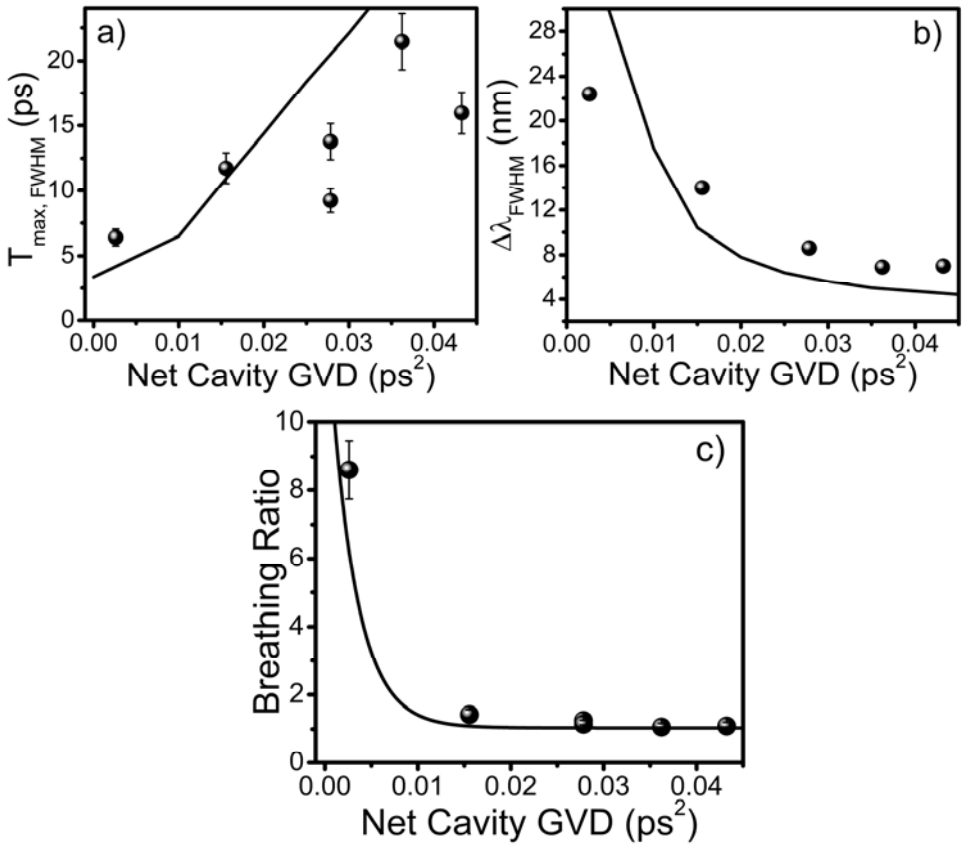

Figure 3.4 (a) Maximum chirped pulse duration (from NPE output) versus net GVD. (b) Corresponding spectral bandwidth versus GVD. (c) Intra-cavity breathing ratio versus GVD. In all figures, measured data correspond to the spheres and simulation corresponds to the solid lines.

Figure 3.4(a) shows the output pulse duration versus cavity dispersion. The pulse duration is seen to increase with GVD, and the measured data roughly follows the simulated trend. The major exception is the measurement at 0.044 ps^2, which is about a factor-of-three narrower than what is predicted by simulation. Two likely sources of this discrepancy are pulse shaping due to the gain medium and NPE. Pulse shaping due to gain dispersion is expected to be stronger at large normal GVD. In simulation, gain is modeled as having a parabolic frequency dependence, although the real gain spectrum is likely to be more complicated. NPE is modeled as a single transfer function, when in

reality it is distributed throughout the laser. Figure 3.4(b) shows the output spectral bandwidth versus cavity GVD. The agreement is good at large normal GVD. However, near zero GVD, the measured bandwidth is shorter than simulation by about a factor of 2. It should be noted that the measured bandwidths are somewhat misleading because the corresponding spectra [shown in Figure 3.2(a)-(e)] do not have the smooth profiles seen in simulation [for example in Figure 3.3(a)-(d)]. The intra-cavity breathing ratio is shown in Figure 3.4(c). Here, experiment fits simulation quite well and clearly illustrates the rapid progression to static pulse evolution beyond ~0.015 ps^2 GVD. The breathing ratio was inferred from the measured chirped and dechirped AC signals along with the known GVD of the dechirp stage and the intra-cavity gratings.

Figure 3.5(a) shows the GVD required to dechirp the output pulses from the NPE port. This is a measure of the chirp on the output pulses. The chirp is seen to increase with increasingly normal GVD. The dechirped pulse duration versus cavity GVD is shown in Figure 3.5(b). In calculating the dechirped duration, the TOD of the dechirp gratings was accounted for. Of key importance here is the fact that these highly chirped, ~ 10- to 20-ps pulses can be dechirped to < 200 fs. The pulse quality versus GVD is shown in Figure 3.5(c). Even at large GVD, the dechirped pulses are within 1.8 times transform limit.

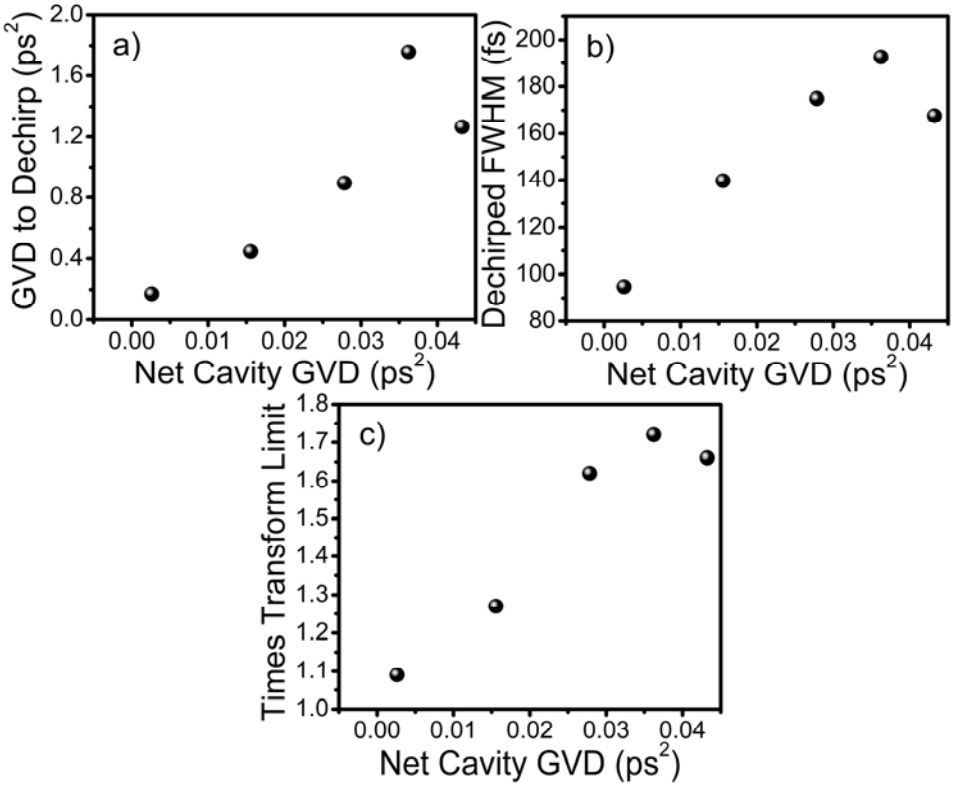

Figure 3.5 (a) GVD required to dechirp pulses from NPE port. (b) Dechirped pulse duration accounting for the TOD imparted by the dechirp grating pair. (c) Pulse quality defined as times transform limit taking into account the TOD of the dechirp grating pair.

The primary motivation for operating at large normal GVD is to produce high-energy pulses. Consequently, it is instructive to explore the maximum output pulse energy versus cavity GVD. Simulations predict an exponential increase in self-similar pulse energy with increasing GVD (Reference [2]). Figure 3.6 compares these simulations to measured data for this laser.

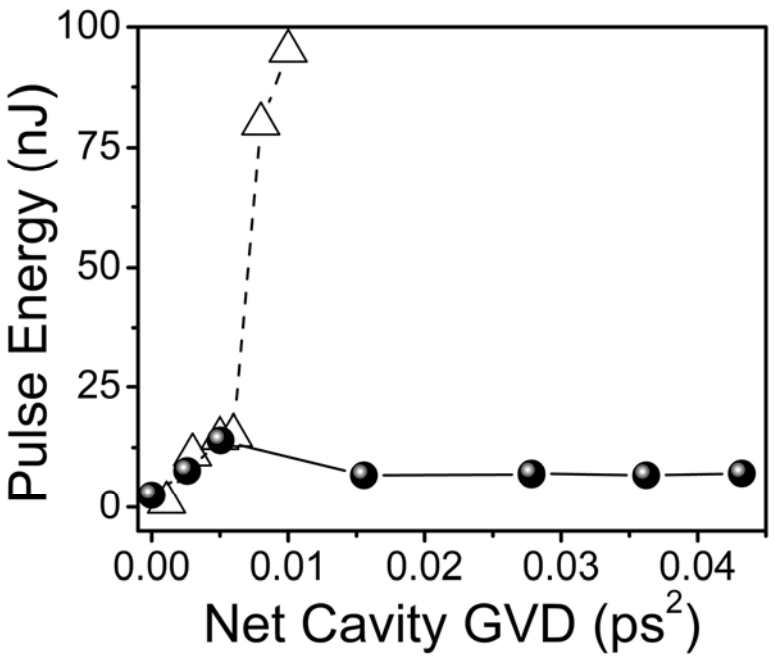

Figure 3.6 Maximum pulse energy versus net cavity GVD. (triangles = simulation, boxes = measured).

The agreement between simulation and experiment is excellent out to ~0.005 ps^2. Beyond this, the experimental pulse energy is capped at ~ 7 nJ, whereas simulation predicts energies that surpass 100 nJ. Admittedly, it takes care to achieve greater than 10-nJ pulse energies in experiment, and our measurements beyond 0.005 ps^2 may not represent the highest attainable energies from this laser. Nevertheless, the general trend clearly indicates a discrepancy with the simulations, which predict a rapid increase in pulse energy with increasingly normal GVD. A possible explanation for this discrepancy is that the pulse energy is limited by over-driving the artificial saturable absorber. Several observations support this claim. The highest pulse energies are obtained by first modelocking the laser with a lower-energy mode, then adjusting the waveplates (thus shifting NPE) until modelocked operation is no longer self-starting. This suggests that the highest energies are obtained

by biasing NPE very close to the over-driving point where self-starting operation is very weak. Furthermore, we investigated the effects of increasing the SMF after the Yb gain fiber (effectively increasing nonlinear phase accumulation and thus NPE). We find that, as the SMF increases, the maximum attainable pulse energy decreases. This suggests that increasing the SMF after the gain pushes the NPE rollover point to lower pulse energy.

Given the agreement between simulation and experiment (excepting the pulse energy measurements beyond GVD ~ 0.005 ps^2), we are inclined to believe the highly chirped pulses which exist at GVD > ~0.015 ps^2 represent a limit of self-similar operation at large normal GVD. This conclusion is supported by the fact that the measured pulse evolution and maximum pulse energy closely resembles self-similar operation.

3.4 A new pulse evolution for fiber lasers

In changing the net cavity GVD from roughly zero to large normal (~0.040 +/- 0.002 ps^2), the pulse evolution changes drastically. The effective SPM felt by the pulse decreases by a factor of 5 (based on measurements of the power reflected off the first cavity grating), whereas the effective GVD felt by the pulse decreases by a factor of 1800 (estimated by calculating the linear propagation of a chirped m=2 super Gaussian pulse inside the SMF portion of the laser). Clearly, the pulse dynamics are no longer determined by an interplay between GVD and SPM as in soliton, stretched-pulse, wave-breaking-free, and self-similar evolutions. It is appropriate to delineate this new form of evolution in fiber lasers as chirped-pulse propagation, as it has

been called in solid-state lasers under similar conditions (Reference [4]). Similar observations have recently been obtained with an erbium-doped fiber laser operating at very large normal GVD (~0.2 ps^2) [12]. The output pulses from this laser were found to have very poor quality and could only be dechirped from ~ 21 ps to 17 ps in duration. Also, the pulse energy was only ~ 0.55 nJ. The authors refer to the pulse evolution as being a form of soliton propagation. However, strictly speaking, this is not the case given that there is no balance between GVD and SPM.

3.5 Comparison to analytic theory

Analytic theory for APM predicts long, highly chirped pulses at large normal GVD and describes pulse-shaping as an interplay between SPM and gain dispersion (References [7] and [8]). In this regime, gain bandwidth filtering translates into amplitude modulation, assisting NPE. Inherent in this theory is the assumption of small pulse changes per pass. Although gain and loss in our cavity represent large perturbations, the fact that the resulting chirped pulse solutions are almost static in time and frequency motivates us to compare our measurements with the theory.

By treating all the pulse-shaping effects as small perturbations, Haus and co-workers were able to describe an APM laser cavity using a relatively simple master equation, first given in Reference [7], as follows:

$$\left[-j\Psi - (l + jx) + g\left(1 + \frac{1}{\Omega_g^2}\frac{d^2}{dt^2}\right) + jD\frac{d^2}{dt^2} + (\gamma - j\delta)|a|^2 \right] a = 0 \quad (3.1)$$

In this equation, g is the amplitude gain coefficient, and Ω_g is the gain bandwidth. The term multiplied by Ω_g describes gain dispersion. The term multiplied by D describes GVD; γ is the self-amplitude modulation (SAM) term, and δ is the SPM term. The term (l + jx) represents the linear loss and phase shift that a pulse experiences per pass, and ψ is a small carrier frequency phase shift. To lowest order, the gain of the laser can be set equal to the linear loss. All of the terms are de-coupled, and the operators represent changes to the pulse amplitude, a, during one cavity round trip. Equation (3.1) represents the fact that, in the steady-state, all changes in one round trip must cancel. Equation (3.1) has an analytic solution of the form:

$$a = A\operatorname{sech}\left(\frac{t}{\tau}\right)e^{\left[j\beta \ln \operatorname{sech}\left(\frac{t}{\tau}\right)\right]} \qquad (3.2)$$

where A is the pulse envelope amplitude, τ is the 1/e intensity duration, and β is the chirp parameter. Substituting (3.2) into (3.1), expressions can be obtained for β, τ, and the spectral bandwidth

$$\omega = \frac{\sqrt{1+\beta^2}}{\tau} \qquad (3.3)$$

in terms of the normalized dispersion parameter D, the SAM coefficient γ and the SPM coefficient δ.

Our Yb fiber laser is modeled as having a parabolic gain with a 1/e gain bandwidth of 30 nm. The SPM and SAM coefficients are modeled using expressions developed by Kohichi Tamura which describe NPE as a function

of the relative angles of the quarter- and half-wave plates in our laser [13]. The SPM coeffiecient is derived assuming 6 m of SMF with a 3-μm mode-field. The pulse energy after the Yb gain was set to 7.8-nJ, corresponding to experiment. The wave plate angles were aligned to provide reasonable values for γ and δ and to provide the same linear loss that we measure through the NPE port (about 90% loss, which admittedly violates one of the assumptions behind the model).

Figure 3.7 compares measurement to theory. Figure 3.7(a) plots the pulse duration versus net GVD. Because the theory assumes negligible changes per round trip, there is an inherent ambiguity when comparing to measurement. In experiment, the pulse always changes to some degree during one round trip, and it is unclear at which point in the cavity one should compare the pulse duration to the theory. For this reason, Figure 3.7(a) plots both the minimum and maximum durations at each GVD. Figure 3.7(b) plots spectral bandwidth versus GVD.

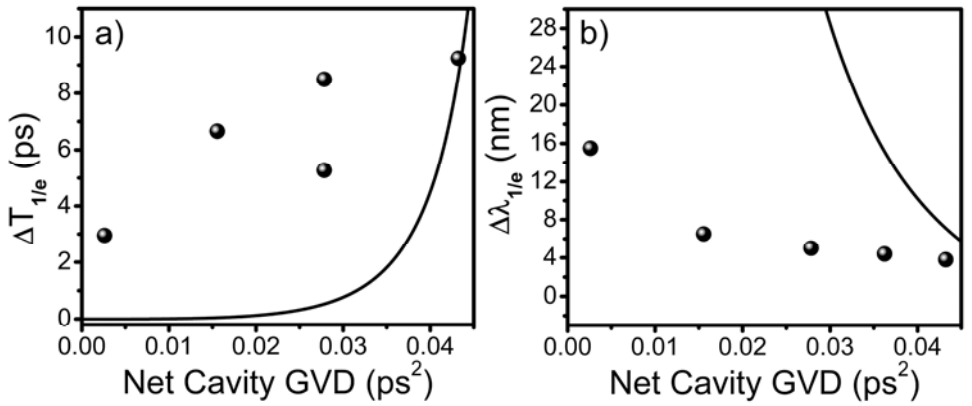

Figure 3.7 (a) Pulse duration versus net cavity GVD (large sphere = measured at maximum duration, small sphere = measured at minimum duration, solid line = analytic theory). (b) Modelocked spectral bandwidth versus net cavity GVD (spheres = measured, solid line = analytic theory).

Theory predicts an exponentially increasing duration with GVD. Likewise, the bandwidth is predicted to rapidly decrease with GVD. Unfortunately, the agreement between experiment and theory is not very good, especially near zero GVD. In retrospect, the lack of agreement is not too surprising. At small GVD values, the pulse breathes heavily which violates the assumption of small pulse changes per pass. Moreover, the gain and loss in the experimental system are quite large; whereas, the analytic theory requires these terms to be perturbations in order to decouple them from the pulse evolution.

3.6 Conclusions and acknowledgements

In conclusion, we have demonstrated for the first time to our knowledge, a new regime of pulse evolution in femtosecond fiber lasers. We refer to this as chirped-pulse propagation, following similar designations for solid-state lasers operating at net normal GVD (Reference [4]). It must be stressed that these chirped-pulse solutions are not trivial in that the nonlinear phase accumulated per round trip is appreciable and is of the same magnitude as experienced during soliton operation. However, chirped-pulse evolution is distinct from soliton operation in that the GVD and SPM are not balancing each other. In fact, GVD effects are negligible, and the pulse-shaping forces are expected to result from a combination of SPM, gain bandwidth filtering, and NPE. When compared to simulations of self-similar fiber lasers, these chirped-pulse modes appear to be a limit of self-similar operation at large normal GVD. Although the simulations predict an exponential increase in energy with GVD, experiments indicate that the maximum energy of 14-nJ occurs at roughly 0.005 ps^2. Beyond that, the energy is at best limited by this value. The likely

limitation is overdriving NPE. Finally, our measurements are compared to the analytic theory. Although the quantitative agreement is not good, the predicted qualitative trends are observed.

Portions of this work were supported by the NIH, and NSF-ECS. The work in this chapter was performed with Andy Chong.

BIBLIOGRAPHY

[1] D. Anderson, M. Desaix, M. Karlsson, M. Lisak, and M.L. Quiroga-Teixeiro, "Wave-breaking-free pulses in nonlinear-optical fibers," J. Opt. Soc. Am. B **10**, 1185 (1993).

[2] F.Ö. Ilday, J.R. Buckley, W.G. Clark, F.W. Wise, "Self-Similar Evolution of Parabolic Pulses in a Laser," Phys. Rev. Lett. **92**, 3902 (2004).

[3] S.H. Cho, F.X. Kärtner, U. Morgner, E.P. Ippen, J.G. Fujimoto, J.E. Cunningham, and W.H. Knox, "Generation of 90-nJ pulses with a 4-MHz repetition-rate Kerr-lens mode-locked Ti:Al_2O_3 laser operating with net positive and negative intracavity dispersion," Opt. Lett. **26**, 560 (2001).

[4] A. Fernandez, T. Fuji, A. Poppe, A. Fűrbach, F. Krausz, and A. Apolonski, "Chirped-pulse oscillators: a route to high-power femtosecond pulses without external amplification," Opt. Lett. **29**, 1366 (2004).

[5] B. Proctor, E. Westwig and F. Wise, "Characterization of a Kerr-lens mode-locked Ti:sapphire laser with positive group-velocity dispersion," Opt. Lett. **18**, 1654 (1993).

[6] J.M. Dudley, S.M. Boussen, D.M.J. Cameron and J.D. Harvey, "Complete characterization of a self-mode-locked Ti:sapphire laser in the vicinity of zero group-delay dispersion by frequency-resolved optical gating," Appl. Opt. 38, 3308 (1999).

[7] H. A. Haus, J. G. Fujimoto, and E. P. Ippen, "Analytic theory of additive pulse and Kerr lens mode locking," IEEE J. Quantum Electron. **28**, 2086 (1992).

[8] H.A. Haus, J.G. Fujimoto, and E.P. Ippen, "Structures for additive pulse mode locking," J. Opt. Soc. Am. B **8**, 2068 (1991).

[9] M. Hofer, M. E. Fermann, F. Harberl, M. H. Ober, and A. J. Schmidt, "Mode locking with cross-phase and self-phase modulation," Opt. Lett. **16**, 502 (1991).

[10] K. Tamura, J. Jacobson, H.A. Haus, E.P. Ippen, and J.G. Fujimoto, "77-fs pulse generation from a stretched-pulse mode-locked all-fiber ring laser," Opt. Lett. **18**, 1080 (1993).

[11] F.Ö. Ilday, J.R. Buckley, H. Lim, F.W. Wise, and W.G. Clark, "Generation of 50-fs, 5-nJ pulses at 1.03 microns from a wave-breaking-free fiber laser," Opt. Lett **28**, 1365 (2003).

[12] L.M. Zhao, D.Y. Tang, and J. Wu, "Gain-guided soliton in a positive group-dispersion fiber laser," Opt. Lett. **31**, 1788 (2006).

[13] K. Tamura thesis

Chapter 4

Stabilization of high-energy femtosecond ytterbium fiber lasers by use of a frequency filter

4.1 Introduction

In Chapter 2, experiments are reviewed in which the maximum attainable pulse energy from an Yb fiber laser is 14 nJ, and the evidence suggests the artificial saturable absorber (NPE in this case) is the primary limitation to achieving higher energies. Experiments performed in Chapter 3 support this idea. For example, the measured self-similar pulse energy versus cavity GVD deviates significantly from simulations which model NPE as monotonic function (Figure 3.6). An obvious way to circumvent this problem is to not use NPE at all, for example by using a real saturable absorber in the laser. This will be discussed somewhat in Chapter 6. Suffice it to say, it is difficult to achieve high-quality femtosecond pulses in fiber lasers without an artificial saturable absorber such as NPE. This is due to the virtually instantaneous response time and strong amplitude modulation that are characteristics of NPE.

In this chapter, we investigate the role of NPE in limiting the maximum pulse energy attainable from femtosecond fiber lasers. By reducing the strength of the NPE, and using an intra-cavity frequency filter to stabilize mode-locked operation at large normal group-velocity dispersion (GVD), we

are able to generate 55-fs pulses with 130 kW peak power. At the time of this writing, this constitutes a record peak power for a femtosecond fiber oscillator. Of equal importance, the stability of this laser at the highest pulse energies is greatly enhanced over what is reported in Chapter 2, which makes this laser a useful tool for applications.

4.2 Investigating the effects of NPE in a fiber laser

Theoretically, the self-similar pulse energy increases with increasing net cavity GVD [1], and this motivates investigation of operation with large normal GVD. The Yb fiber laser setup shown in Figure 4.1 is similar to that discussed in Chapter 2. Mode-locking is initiated through NPE controlled by two quarter- and one half-wave plates. The output is taken from the NPE rejection port of the polarizing beam cube. A knife edge can be positioned inside the spectrally-dispersed beam (Figure 4.1) to act as a spectral filter. For all mode-locked states of operation, the laser produces positively-chirped pulses, which are dechirped with a grating pair external to the cavity.

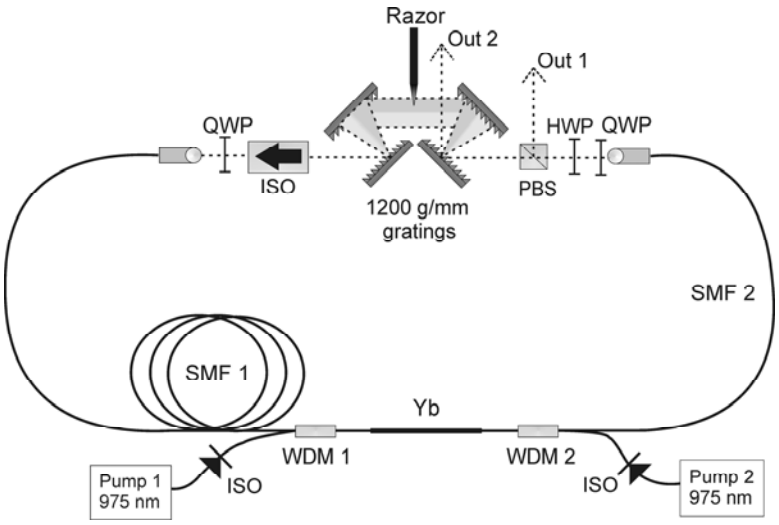

Figure 4.1 Yb fiber laser setup. SMF: single-mode fiber, QWP: quarter wave plate, HWP: half wave plate, PBS: polarizing beam splitter, ISO: isolator, WDM: fiber-pigtailed coupler.

Working under the assumption that overdriving the NPE limits the pulse energy, we attempted to design a laser in which the overdriving point occurs at highest pulse energy. This is shown schematically in Figure 4.2 below.

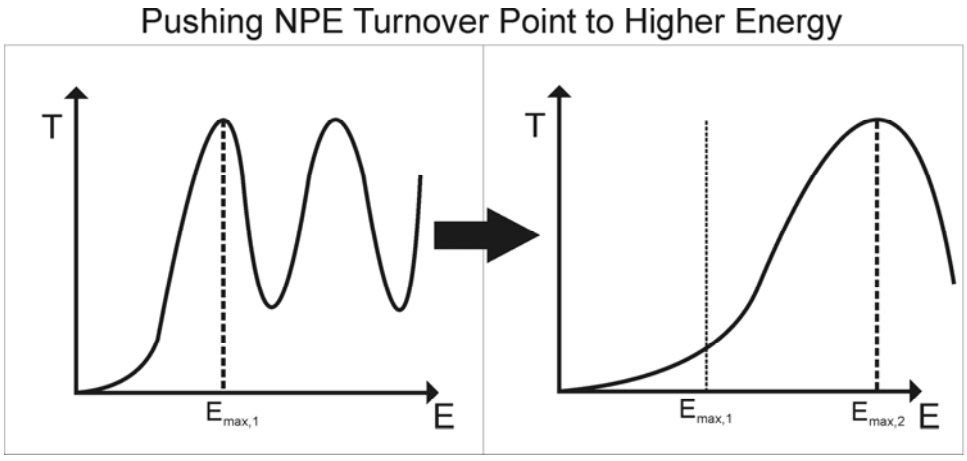

Figure 4.2 Cartoon showing saturable absorber action due to NPE. The curve on the left has a turnover point at Emax,1 which is at lower energy than the same point for the curve on the right (labeled Emax, 2).

Because loss in the open-air section of the laser can be as high as 20 dB, the majority of the nonlinear phase (and thus NPE action) accumulates within the segment of SMF (labeled "SMF2" in Figure 4.1) that follows the Yb-doped gain fiber. By minimizing this length of fiber, we expect to reduce the strength of NPE while simultaneously pushing the overdriving energy higher.

As a control experiment, the laser was initially operated without the knife edge in the cavity. The length of SMF2 was varied from a minimum of 37 cm (determined by the practical need to have a fiber coupler and collimator at this location) to a maximum of 9 m. The performance of the laser was found to depend strongly on the length of SMF2. The threshold for modelocking decreased with increasing length of SMF2. This observation is consistent with the expectation that, for a given mode-locked state, increasing the length of SMF2 increases the strength of NPE.

Increasing the length of SMF2 increased the range of normal GVD over which mode-locked operation was stable. At the minimum length of 37 cm, stable operation was attainable only for net GVD up to 0.005 +/- 0.002 ps^2. When the length of SMF2 was increased to 1 m, stable operation extended out to ~0.040 ps^2, and with 3 m, mode-locking could be obtained out to ~0.100 ps^2. When net GVD is increased, the output pulse duration and chirp substantially increase. Long, highly-chirped pulses will experience less amplitude modulation from NPE than shorter pulses. Consequently, we attribute the failure of mode-locking at large normal GVD to a failure of NPE action. Because lengthening SMF2 extends the operational range of GVD, we conclude that increasing SMF2 strengthens NPE pulse shaping.

The maximum stable pulse energy of ~10 nJ occurs when SMF2 is ~1 m long. For shorter lengths, the pulse energy is believed to be GVD-limited. When SMF2 is too short, the largest normal GVD at which stable operation can be achieved lies closer to zero. This smaller GVD cannot balance very large nonlinear phase shift and avoid wave-breaking (Reference [1]). When SMF2 is too long, even moderate pulse energies result in excessive nonlinear phase which overdrives the NPE.

4.3 A fiber laser with reduced NPE

These experimental observations support the conclusion that NPE is dominated by the length of SMF following the gain fiber. Additional experiments confirm that the laser performance is relatively independent of the length of fiber *before* the Yb gain (labeled "SMF1" in Figure 4.1). Motivated to obtain the highest pulse energies, we reduce the length of SMF2 to the minimum of 37 cm. To stabilize mode-locking at larger net GVD, where we expect the highest pulse energies, additional self-amplitude modulation that is independent of NPE will be needed. Numerical simulations of self-similar pulse evolution (Reference [1]) show that significant amplitude modulation arises from spectral clipping of the chirped pulse in the gain medium. Frequency is mapped to time in a highly-chirped pulse, so attenuation of the edges of the spectrum attenuates the temporal wings of the pulse. Our goal is to increase the strength of this process, which might allow a corresponding reduction in the strength of the NPE. The knife-edge is a simple experimental implementation of a filter.

Experimentally, a razor blade is mounted on a translation stage, and different mode-locked spectra are generated by moving it in and out of the beam. Loss induced by the razor is easily recovered by the Yb gain, and the efficiency of the laser is unchanged. By simultaneously adjusting the NPE waveplates and the spectral filter, stable mode-locked operation can be reproducibly achieved out to a net GVD of 0.015 ps^2. Without the razor, mode-locking is limited to a net GVD less than 0.005 ps^2. The highest pulse energies were obtained with the maximum net GVD. The best results are generally achieved when the razor blocks the short-wavelength portion of the spectrum.

Beginning with no spectral filtering, the razor is inserted into the spatially dispersed beam (Figure 4.1) in increments of ~ 0.1 mm. At each step, the waveplates are adjusted in an attempt to modelock the laser. This procedure is repeated at increasing values of net GVD with the goal of generating pulses at large normal GVD. Figure 4.3 shows data taken at a net GVD of 0.015 +/- 0.002 ps^2, where some degree of spectral filtering is needed to achieve stable modelocked operation. Figure 4.3(a) shows the spectrum rejected from the NPE port (solid line) and the spectrum of the intra-cavity pulse (dashed line) on a semi-log scale. Stable single-pulsing is verified with a fast detector down to 500 ps, and with interferometric autocorrelation out to ~100 ps. Also, the spectrum is carefully monitored for any modulation that would be consistent with multiple pulses in the cavity. By measuring the GVD required to dechirp the output pulses, the pulse evolution is determined to breathe with a minimum duration inside the SMF shifted about 1 m from the center of the fiber. The repetition rate is 20 MHz, and the average output power is 330 mW, resulting in 16.5 nJ of pulse energy.

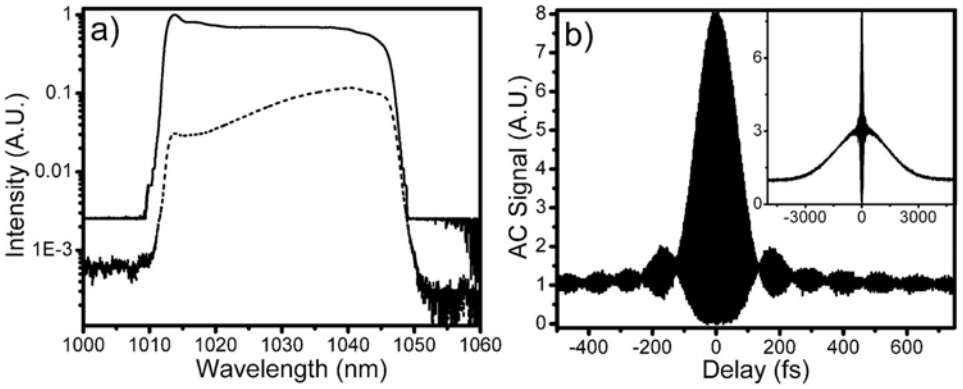

Figure 4.3 (a) Spectrum of pulses from NPE rejection port (solid) and from pulses circulating inside the cavity (dotted). (b) Interferometric autocorrelations of chirped (inset) and dechirped pulses from NPE port.

This initial result represents an 18% improvement in pulse energy over what is reported in Chapter 2. More importantly, modelocked operation is very stable and self-starting. Over a period of one day, the laser was shut down and powered up several times, each time returning to the same high-energy, single-pulsing mode. Evidently, the added amplitude modulation due to the spectral filter assists NPE in starting and stabilizing modelocked operation. Autocorrelations of the output pulses are shown in Figure 4.3(b). The chirped output pulse duration is 2.5 ps. The dechirped pulse duration is 98 fs, which is ~25% beyond transform limit.

Further insertion of the razor blade actually produces a broader output spectrum, shown in Figure 4.4(a). The oscillatory structure on the short-wavelength side of the spectrum coincides with the position of the razor blade in the spatially-dispersed beam, and is reminiscent of the Fresnel diffraction pattern cast by a knife edge. The intra-cavity pulse evolution is wave-breaking-free, with the minimum pulse duration occurring near the end of the SMF. The

pulse autocorrelations are shown in Figure 4.4(b). The chirped pulse energy from the NPE port is measured to be 13.1 nJ, corresponding to 265-mW average power, and the pulse duration is 2 ps. After dechirping, the pulse duration is ~60 fs.

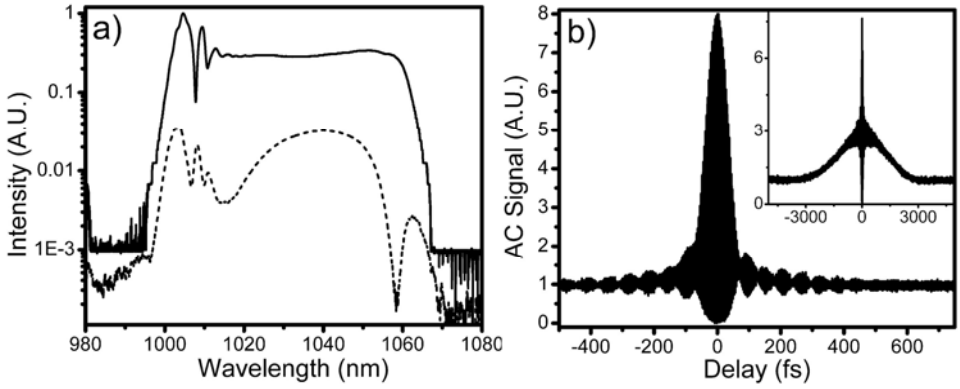

Figure 4.4 (a) Spectrum of pulses from NPE rejection port (solid) and from pulses circulating inside the cavity (dotted). (b) Interferometric autocorrelations of chirped (inset) and dechirped pulses from NPE port.

The intensity and phase of the dechirped pulse is inferred using a pulse retrieval algorithm based on fitting the measured interferometric autocorrelation and spectrum [2]. Figure 4.5 shows the result of this fit. The good agreement between the measured [Figure 4.5(a)] and retrieved [Figure 4.5(b)] autocorrelations gives us confidence in the results. The FWHM pulse duration is 55-fs, which is about 20% larger than the transform-limited duration. Integrating over the intensity profile of the dechirped pulses results in a peak power of 130 kW, assuming an 80% dechirping efficiency which is achievable with highly efficient diffraction gratings (95% single-pass efficiency) or photonic bandgap fiber (80% coupling efficiency). Although the pulse energy is lower than that of Figure 4.3, the peak power is slightly higher owing to the shorter pulse duration.

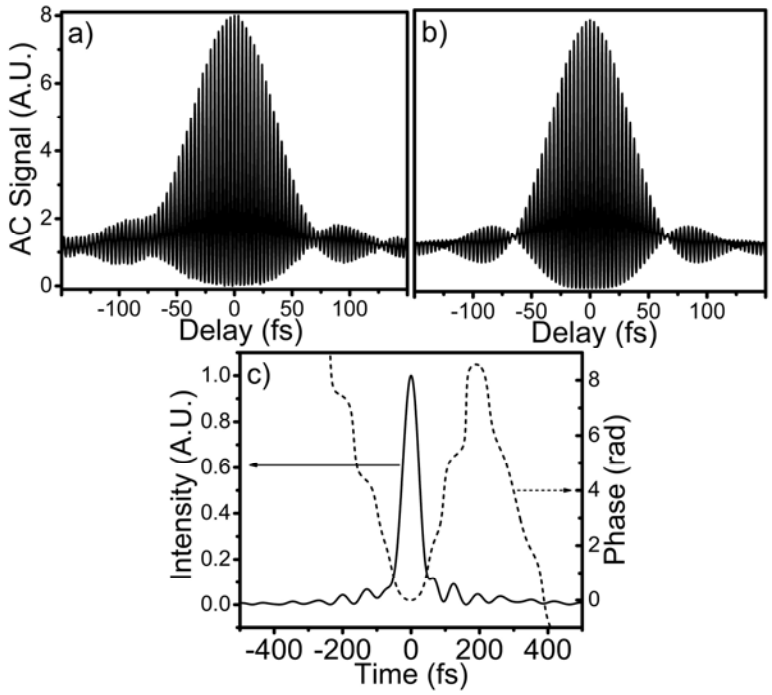

Figure 4.5 (13.1-nJ pulses) (a) Measured autocorrelation of dechirped pulse. (b) Calculated autocorrelation of retrieved pulse. (c) Retrieved pulse intensity (solid) and phase (dashed) profiles.

4.4 Measurements of NPE action in spectrum and time

By observing the differences between the spectrum rejected and accepted by the NPE port, one can assess the relative strength of NPE pulse shaping in the cavity. For all modes of pulse evolution at net-normal GVD, the pulses are highly chirped at the NPE rejection port. As a result, the pulse spectrum is mapped to the time domain, and strong pulse shaping is expected to coincide with strong spectral shaping. Figure 4.6 shows rejected (solid) and accepted (dashed) spectra for three different modes of evolution. These spectra have been scaled by their respective energies. Figure 4.6(a) corresponds to the highest peak power. The evolution is wave-breaking-free with a pulse

minimum near the Yb gain at the end of the SMF fiber. Figure 4.6(b) corresponds to the highest pulse energy, where the pulse minimum is shifted closer to the center of the SMF segment. Figure 4.6(c) is data taken from the laser in self-similar operation. Self-similar evolution is not found to be stable under the conditions necessary for the highest peak power and energy.

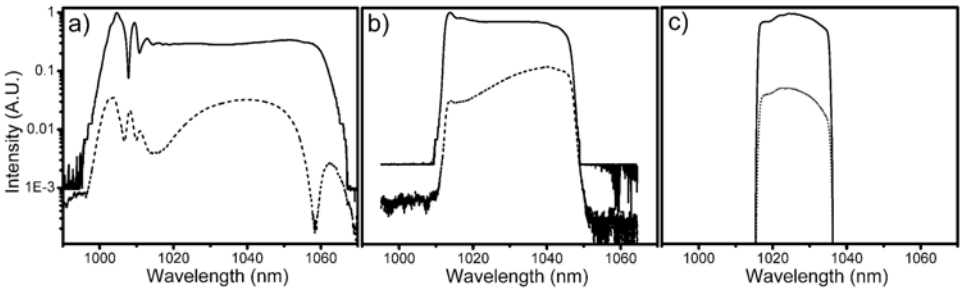

Figure 4.6 (a) Spectra corresponding to highest peak power. (b) Spectra corresponding to highest pulse energy. (c) Spectra from self-similar laser with about 1 m of SMF after the Yb gain fiber. In all figures the solid line is the output spectrum and the dashed line is the spectrum inside the cavity.

Consequently, Figure 4.6(c) depicts modelocked spectra from a different Yb fiber laser, and it is shown here to illustrate a qualitative trend. Moving from left to right in Figure 4.6, the strength of NPE is observed to decrease, whereas the pulse energy increases from Figure 4.6(a) to Figure 4.6(b) and would presumably increase further in going from Figure 4.6(b) to Figure 4.6(c). This presumption is based on the observation that the same laser which produces Figure 4.6(a) and Figure 4.6(b), produces the highest output powers when it is close to operating in the self-similar mode (evidenced by a stable spectrum with an unstable pulse train). We conclude that the highest pulse energies are achieved by reducing the strength of NPE, which helps to avoid overdriving the artificial saturable absorber.

A measurement of NPE action in the time domain is achieved by comparing the dechirped autocorrelation of pulses from the NPE port (labeled "Out 1" in Figure 4.1) to the autocorrelation of pulses reflected from a cavity grating (labeled "Out 2" in Figure 4.1). The latter autocorrelation is a direct measurement of the pulses circulating inside the cavity. Figure 4.7 shows this comparison, where it can be seen that the pulses circulating inside the laser have significantly less secondary structure than the pulses rejected by NPE (Because an autocorrelation measurement is proportional to the square of pulse intensity, the differences in the wings of the actual pulses are even more pronounced).

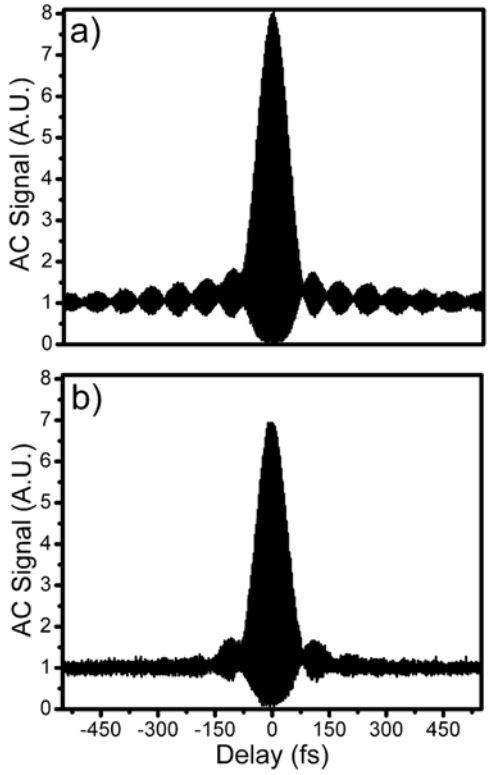

Figure 4.7 (a) Autocorrelation signal for de-chirped pulses from NPE rejection port. (b) Autocorrelation signal of dechirped pulses circulating in cavity.

4.5 Additional observations

At this point, a few observations are worth noting. When the laser generates the highest peak powers, it is not self-starting. To reach this mode, a lower-power, self-starting mode is first attained with the razor blade at a fixed insertion. Then, one or more waveplates are rotated slightly to increase the energy. At the point of maximum energy, if any waveplate is adjusted further, the mode jumps to multi-pulsing. This suggests that the highest peak powers are obtained by biasing the NPE very close to the rollover point, where its strength is too low to assist self-starting operation. On the other hand, the mode of operation resulting in slightly lower peak power (Figure 4.3) is self-starting. All modes of pulse evolution are found to be highly chirped at the NPE rejection port. As a result, the pulse spectrum is mapped to the time domain, and strong pulse shaping coincides with strong spectral shaping. By observing the qualitative difference between the spectra rejected and accepted by the NPE port, we can assess the relative strength of NPE pulse shaping in the cavity. Comparing Figures 4.3 and 4.4, we conclude that the highest pulse energies are achieved by reducing the strength of NPE, which avoids overdriving it.

The output energy is currently limited by available pump power. Significantly higher pump power will require the use of double-clad fiber. A stretched-pulse laser based on double-clad Yb fiber produced 11.8-nJ chirped pulses (110 mW average power), which were dechirped to 200 fs outside of the laser, although an acousto-optic modulator was needed to assist

modelocking [3]. This result is encouraging, but does not reach the performance of SMF-based lasers reported here. An initial result of 25-nJ chirped pulses (dechirped to ~ 200 fs) from a double-clad Yb fiber laser has recently been reported [4]. To our knowledge, this would represent the highest pulse energy from a fiber laser. However, the resulting peak power would be significantly lower than what is obtained here. Although double-clad fiber lasers lack some of the integration of SMF fiber lasers, the route to higher pulse energy will likely require double-clad architectures, at least in the near future.

4.6 Conclusions and acknowledgements

In conclusion, our investigations support the claim that overdriving NPE is the primary limitation to achieving higher pulse energies from femtosecond fiber oscillators with large normal GVD. By minimizing the length of SMF after the gain fiber, we can push the NPE turnover point to higher pulse energy. The consequent reduction in NPE action is offset by self-amplitude modulation produced by adding a frequency filter to the cavity. With this approach, we are able to generate record peak power (130 kW) from a femtosecond fiber oscillator. These results are routinely achievable, whereas previous work reports that only 5- to 7-nJ pulses are routine [5]. To our knowledge, this is the first fiber oscillator capable of simultaneously generating ~50-fs pulses with ~10-nJ energy.

Portions of this work were supported by the NIH (EB002019), and NSF-ECS. Much of the work in this chapter would not have been possible without the assistance of Andy Chong, Shian Zhou, and Will Renninger.

BIBLIOGRAPHY

[1] F. Ö. Ilday, J.R. Buckley, W.G. Clark, F.W. Wise, "Self-Similar Evolution of parabolic Pulses in a Laser," Phys. Rev. Lett. **92**, 3902 (2004).

[2] J.W. Nicholson, J. Jasapara, and W. Rudolph, "Full-field characterization of femtosecond pulses by spectrum and cross-correlation measurements," Opt. Lett. **24**, 1774 (1999).

[3] A. Albert, V. Coudec, L. Lefort, A. Barthelemy, "High-energy femtosecond pulses from an ytterbium-doped fiber laser with a new cavity design," IEEE P. Tech. Lett. **16**, 416 (2004).

[4] M.J. Messerly, J.W. Dawson, and C.P.J. Barty, "25 nJ Passively Mode-Locked Fiber Laser at 1080 nm," Conference on Lasers and Electro-Optics (CLEO), CThC7, Long Beach, CA (2006).

[5] J.R. Buckley, F. Ö. Ilday, and F.W. Wise, "Femtosecond fiber lasers with pulse energies above 10 nJ," Opt. Lett. **30**, 1888 (2005).

Chapter 5

Generation of ten-cycle pulses from an ytterbium fiber laser with cubic phase compensation*

5.1 Introduction

Chapter's 2 and 4 discussed experiments aimed at maximizing the pulse energy from an ytterbium fiber laser, while Chapter 3 discussed a new form of pulse evolution in fiber lasers which has potential applications for generating high-energy pulses. In this chapter, the focus shifts to two other figures of merit for femtosecond lasers – namely, minimum pulse duration and pulse quality. There is great interest in sources of few-cycle pulses (meaning the intensity envelope covers < 10 optical cycles). Applications involving time-resolved studies demand high-quality, short pulses. Moreover, applications requiring high peak powers can benefit from more stable and compact femtosecond lasers.

* J.R. Buckley, S.W. Clark, and F.W. Wise, Opt. Lett. 31, 1340 (2006).

A typical Ti:sapphire laser produces anywhere from 10- to 20-nJ pulses. The first few chapters of this thesis have shown that fiber lasers are now directly competitive with solid-state lasers in terms of pulse energy at specific wavelengths. However, fiber lasers continue to lag behind in pulse duration. A Kerr-lens modelocked Ti:sapphire laser has produced pulses as short as ~5 fs, or two optical cycles [1]. A similar laser with a saturable-absorbing mirror (SAM) to assist mode locking has achieved roughly the same pulse duration [2]. In contrast, the shortest pulses produced from an Er fiber laser had duration of 63 fs [3], while a Nd fiber laser generated pulses as short as 38 fs [4]. Ilday *et. al.* demonstrated 36-fs pulses from a stretched-pulse Yb fiber laser by optimizing second-order dispersion inside the cavity [5]. However, the pulse quality was low, with significant energy extending out to 150 fs. The primary limitation to achieving shorter pulses was attributed to uncompensated third-order dispersion (TOD) inside the laser cavity.

It is well known that prism pairs can compensate the TOD of optical fiber [6]. For example, Fork *et. al.* were able to generate 6-fs pulses using prisms and gratings in a fiber compressor stage [7]. Kane *et. al.* used a coupled prism-grating sequence to compensate for the residual TOD of a grating stretcher in order to amplify sub-100-fs pulses [8]. Some progress has been made toward reducing TOD inside fiber lasers. Fermann *et. al.* achieved 180-fs pulses from an Er fiber laser using partial TOD compensation from an intra-cavity prism pair [9]. Dispersion-compensating fiber has also been used inside an Er fiber laser for partial TOD compensation [10].

In this work, we demonstrate the capability to fully compensate for the net cavity TOD inside a Yb fiber laser by using a sequence of prisms embedded within a grating pair. The laser performance was investigated as a function of net cavity group velocity dispersion (GVD) and TOD, with the goal of generating pulses of minimum duration. Pulses as short at 33 fs, corresponding to ten cycles, were generated with excellent pulse quality.

5.2 Experiment

Numerical calculations were performed to determine the GVD and TOD imparted on a pulse by various prism-grating geometries. These computations were based on analytic expressions for the dispersion of arbitrary prism sequences [11], along with standard textbook equations for grating-pair dispersion [12]. It was determined that optimal dispersion compensation could be achieved with a prism-grating sequence similar to that reported in Ref.erence [8], in which the prism pair is inserted inside the grating pair. In this configuration, the prism sequence dispersion is greatly amplified by the presence of the gratings.

Several prisms and gratings were investigated in a search for a sequence that could compensate for the dispersion of meters of single-mode fiber (SMF) using short prism-grating separations (a few centimeters). We chose SF11 prisms and gratings with a density of 600 grooves/mm. This combination provides a TOD-to-GVD ratio of ~2 fs, which is roughly the same ratio for the SMF and allows for ideal second- and third-order phase compensation.

We constructed a Yb fiber laser similar to that in Reference [5]. The oscillator (indicated schematically in Figure 5.1) was pumped in-core with a 975-nm fiber-pigtailed diode laser, and lasing occurred at 1030 nm.

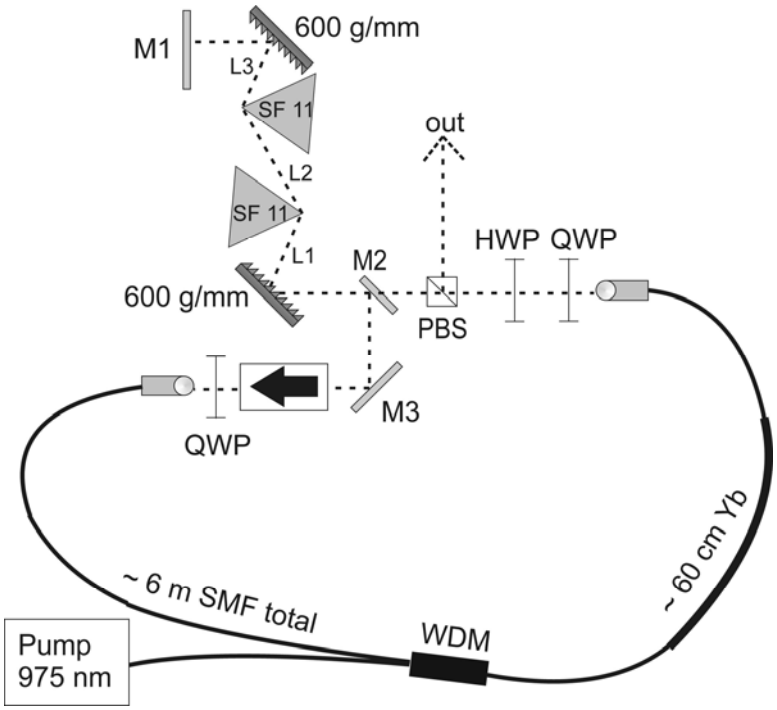

Figure 5.1 Schematic of the fiber laser setup (not to scale). QWP, quarter-wave plate; HWP, half-wave plate; PBS, polarizing beam splitter, M1-M3, mirrors. For the shortest pulses, L1=0.7 cm, L2=9.5 cm, L3=2.1 cm.

Mode locking was initiated and stabilized through nonlinear polarization evolution (NPE), controlled by two quarter- and one half-wave plates. The output was taken directly from the NPE port at the polarizing beam cube. The pulse repetition rate was 29 MHz for the data shown here.

As a control experiment, intra-cavity GVD was compensated for using only a grating pair. This laser architecture has been studied extensively (for example, in Reference [5]). At 1030-nm wavelength, the GVD parameter of the grating

pair (β_2 = -1400 ps^2/km) is the opposite sign of that for the SMF (β_2 ~ 23 ps^2/km), so the grating pair is capable of compensating for the fiber GVD. However, the TOD parameter of the grating pair (β_3 = 2.2 ps^3/km) is the same sign as that of the SMF (β_3 ~0.041 ps^3/km); therefore, the TOD of the grating pair adds to that of the fiber. Figures 5.2(a) and (b) show the spectrum and interferometric autocorrelation respectively, of the shortest pulses generated from this laser. The net cavity GVD was -0.01 +/- 0.002 ps^2. The net TOD of the laser cavity was roughly 0.00044 ps^3. The uncompensated cubic phase set the lower limit on full-width-at-half-maximum (FWHM) pulse duration at roughly 40 fs [55-fs FWHM autocorrelation as shown in Figure 5.2(b)], with significant energy in the pulse wings extending out to ~400 fs. These results are similar to the shortest pulses generated in Reference [5].

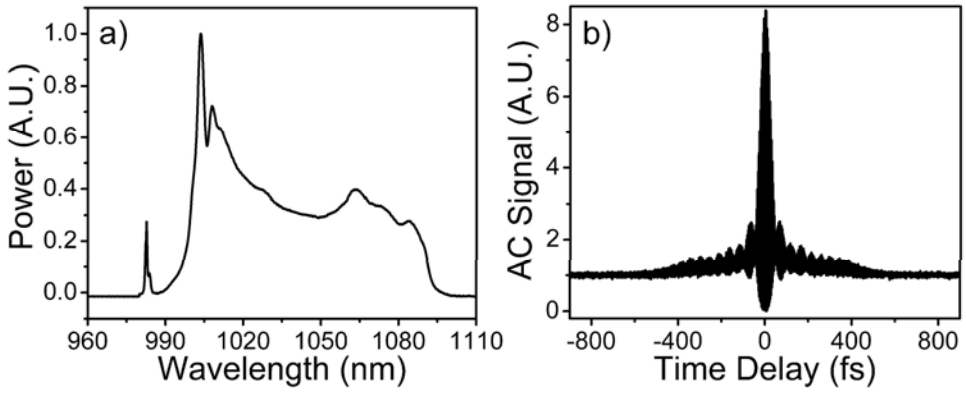

Figure 5.2 (a) Power spectrum of shortest pulses from laser without prisms for TOD compensation. (b) corresponding dechirped autocorrelation.

Next, we incorporated SF11 prisms between the gratings as depicted in Figure 5.1. With the relative prism-grating orientations shown in Figure 5.1, the sequence is capable of producing anomalous GVD and negative TOD, which are the opposite signs of the dispersion of SMF at the operating

wavelength of 1030 nm. (When the prisms apexes point the opposite direction as shown, the resulting sequence adds to the TOD of the fiber.) To reduce cavity losses, the prisms were oriented at Brewster's angle (~60-degree incidence for SF11 at 1030 nm). The laser modelocked and was self-starting over a large range of net-cavity GVD and TOD. We varied the net-cavity GVD and TOD by adjusting the distances between the prisms and gratings. At large values of net GVD, where net TOD was expected to have negligible effect, the laser performed much like in Reference [5]. At large anomalous dispersion, spectra and autocorrelations consistent with soliton propagation were observed. At normal dispersion, stretched-pulse operation was observed. At all values of net-cavity dispersion, the laser produced positively-chirped pulses, which were dechirped external to the cavity using a prism-grating sequence similar to the intra-cavity sequence. The shortest pulses did not correspond to the broadest spectra, which evidently had some uncontrollable phase. The largest spectral bandwidths were achieved with a calculated net GVD of roughly -0.13 ps^2 and net TOD of about -0.00008 ps^3. Typically these spectra were greater than 100-nm at the base, with the largest being up to 130-nm at the base. Figure 5.3 shows data for the shortest pulses, which were initially measured to occur with a net GVD of roughly -0.09 ps^2 and net TOD of -0.00004 ps^3.

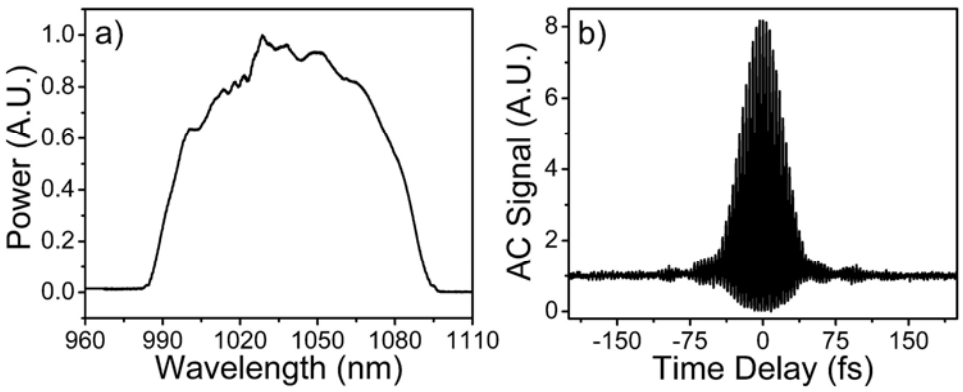

Figure 5.3 (a) Power spectrum of shortest pulses from laser without prisms for TOD compensation. (b) corresponding dechirped autocorrelation.

Error in the measured values of net GVD and TOD was dominated by the uncertainty in the angle of incidence on the second prism. Estimated measurement errors are +/- 0.01 ps^2 in GVD and +/- 0.00002 ps^3 in TOD. Simulations of the laser without prisms predict the broadest spectra and shortest pulses will occur near zero net cavity GVD (Reference [5]). The measured GVD values corresponding to the broadest spectra and shortest pulses were significantly more anomalous than expected from these simulations.

Motivated by this discrepancy, we independently measured the GVD of our prism-grating sequence. We propagated a seed pulse from another laser through the sequence and measured the interferometric autocorrelation before and after the sequence for different prism-grating separations. Prior to passing through the sequence, the seed pulse was within 20% of its transform-limited duration. The measurements indicate the sequence imparts a GVD that is roughly a factor of two smaller in magnitude than expected from calculations. While this is somewhat surprising to us, a possible source of this discrepancy

is the fact that our calculations do not include fourth-order and higher dispersion terms, which become increasingly significant at the very broad bandwidths corresponding to the shortest pulses. Taking into account a factor-of-two correction to the sequence GVD and estimating the same correction to the sequence TOD, the broadest spectra occur with a net GVD of 0 +/- 0.01 ps^2 and with a net TOD of +0.00008 +/- 0.00002 ps^3. The shortest pulses were measured with a net cavity GVD of +0.02 +/- 0.01 ps^2 and with a net TOD of +0.0001 +/- 0.00002 ps^3, representing a factor-of-4 reduction in net TOD over the same laser with only a grating pair for dispersion compensation. The shortest pulses and broadest spectra did not occur at zero net TOD as expected; however, this is not too alarming given the uncertainty in our measurements of net GVD and TOD.

Figure 5.4 provides a side-by-side comparison between the laser without and with TOD compensation, and it clearly illustrates the benefits of reducing the net cavity TOD. The spectrum of Figure 5.4(c) is much less structured than in Figure 5.4(a). The resulting autocorrelation has a FWHM of 50 fs. Even more significant than the slightly shorter pulse is the lack of secondary structure in the autocorrelation shown in Figure 5.4(d).

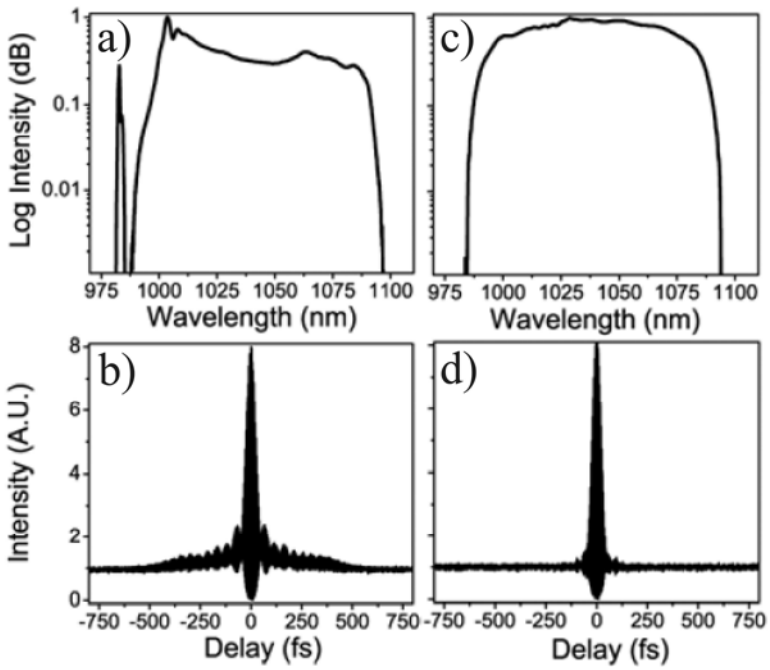

Figure 5.4 (a), (b) Power spectrum and interferometric autocorrelation, respectively, of the shortest pulses from the lasere without TOD compensation. (c), (d) Power spectrum and interferometric autocorrelation of the shortest pulses from the laser with TOD compensation.

The intensity and phase of the shortest pulses were inferred by using a pulse retrieval algorithm (PICASO) based on fitting the measured interferometric autocorrelation and spectrum [13]. Figure 5.5 shows the results of this procedure. Figure 5.5(a) is the measured autocorrelation signal. Figure 5.5(b) is the autocorrelation retrieved by PICASO. Figure 5.5(c) shows the pulse intensity profile and the corresponding phase. The FWHM duration of the pulse is 33-fs, which is within 10% of the zero-phase Fourier transform of the spectrum. The good agreement between the measured and retrieved autocorrelation signals [Figures 5.5(a) and (b) respectively] gives us confidence in the calculated pulse parameters.

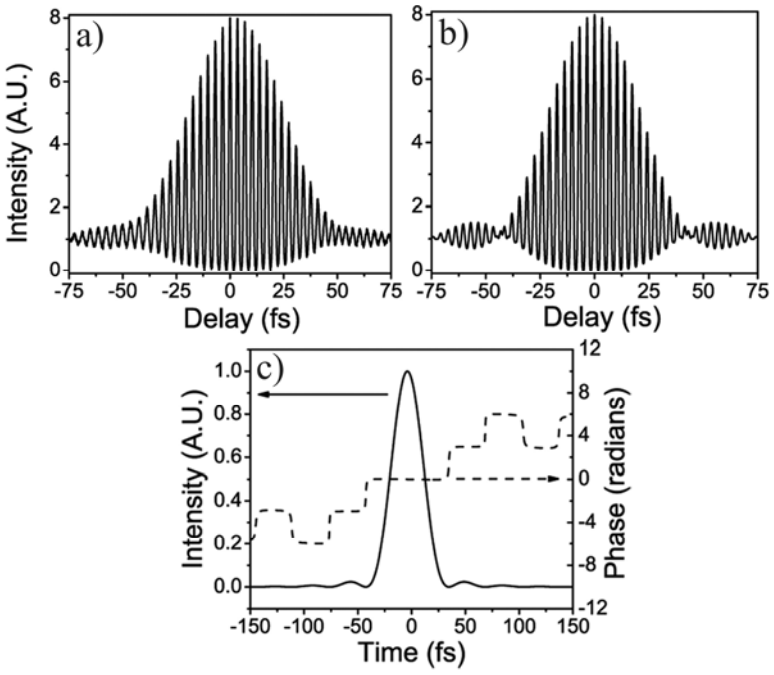

Figure 5.5 (a) Measured dechirped autocorrelation of 33-fs pulses from the laser with TOD compensation. (b) Autocorrelation calculated from the PICASO algorithm. (c) Pulse intensity and phase calculated from PICASO.

Compared to similar fiber lasers without TOD control (Figures 5.4(a) and (b) and Reference [5]), this pulse has excellent quality, with negligible secondary structure in the wings. A common figure of merit for pulse quality is the ratio of energy within one FWHM to that of a Gaussian pulse of the same FWHM duration. The quality of these 33-fs pulses is essentially 1, whereas the quality of the pulses in Reference [5] is about 0.7. To maintain single-pulse operation, the pump power was turned down below 200 mW. The average power coming out of the NPE port was 35 mW, corresponding to 1.2-nJ chirped pulses. No particular care was taken to maximize pulse energy in this experiment. If efficient gratings or photonic bandgap fiber are used to dechirp the pulse, it would be possible to achieve 1-nJ energy and 33-fs duration, which would result in 30-kW peak power.

5.3 Conclusions and acknowledgements

In conclusion, by simultaneously compensating for the GVD and TOD inside a fiber laser, we were able to generate clean, 33-fs pulses, corresponding to ten optical cycles at 1030-nm wavelength. These are what we believe to be the shortest pulses produced from a fiber oscillator to date. With regard to pulse quality, these results constitute a major improvement over the previous shortest pulses from a fiber laser. The use of bulk components to compensate for dispersion in these experiments detracts from some of the benefits of the fiber. Further efforts will address the development of integrated approaches to dispersion control.

This work was performed with Stephen Clark. Portions of this work were supported by the NIH, and NSF-ECS. Ömer Ilday provided valuable discussions. The author acknowledges the support of the National Physical Science Consortium through a graduate research fellowship.

BIBLIOGRAPHY

[1] U. Morgner, F. X. Krtner, S. H. Cho, Y. Chen, H. A. Haus, J. G. Fujimoto, E. P. Ippen, V. Scheuer, G. Angelow, T. Tschudi, "Sub-two-cycle pulsesfrom a Kerr-lens mode-locked Tisapphire laser," Opt. Lett **24,** 411 (1999).

[2] D. H. Sutter, G. Steinmeyer, L. Gallmann, N. Matuschek, F. Morier-Genoud, U. Keller, V. Scheuer, G. Angelow and T. Tschudi, "Semiconductor saturable-absorber mirror assisted Kerr-lensmode-locked Tisapphire laser producing pulses in the two-cycle regime," Opt. Lett. **24,** 631 (1999).

[3] K. Tamura, E. P. Ippen, and H. A. Haus, "Pulse dynamics in stretched-pulse fiber lasers," App. Phys. Lett. **67**, 158-160 (1995).

[4] M. Hofer, M.H. Ober, F. Haberl, and M.E. Fermann, "Characterization of Ultrashort Pulse Formation in Passively Mode-Locked Fiber Laser," IEEE J. Quantum Electron. **28**, 720 (1992).

[5] F.Ö. Ilday, J. Buckley, L. Kuznetsova and F.W. Wise, "Generation of 36-fs pulses from a ytterbium fiber laser," Opt. Express **11**, 3553 (2003).

[6] R.L. Fork, O.E. Martinez, and J.P. Gordon, "Negative dispersion using pairs of prisms," Opt. Lett. **9**, 150 (1984).

[7] R.L. Fork, C.H. Brito Cruz, P.C. Becker, and C.V. Shank, "Compression of optical pulses to six femtoseconds by using cubic phase compensation," Opt. Lett. **12**, 483 (1987).

[8] S. Kane, J. Squier, J.V. Rudd, and G. Mourou, "Hybrid grating-prism stretcher-compressor system with cubic phase and wavelength enability and decreased alignment sensitivity," Opt. Lett **19**, 1876 (1994).

[9] M.E. Fermann, M.J. Andrejco, Y. Silberberg, and A.M. Weiner, "Generation of pulses shorter than 200 fs from a passively mode-locked Er fiber laser," Opt. Lett. **18**, 48 (1993).

[10] M. Dennis and I.N. Duling III, Opt. Lett. **19**, "Third-order dispersion in femtosecond fiber lasers," 1750 (1994).

[11] R.E. Sheriff, "Analytic expressions for group-delay dispersion and cubic dispersion in arbitrary prism sequences," J. Opt. Sco. Am. B, **15**, 1224 (1998).

[12] G.P. Agrawal, *Nonlinear Fiber Optics 2nd Edition* (Academic Press, San Diego, CA, 1995).

[13] J.W. Nicholson, J. Jasapara, and W. Rudolph, "Full-field characterization of femtosecond pulses by spectrum and cross-correlation measurements," Opt. Lett. **24,** 1774 (1999).

Chapter 6

An ytterbium fiber laser modelocked with a semiconductor saturable absorber mirror

6.1 Introduction

In the previous chapters, femtosecond pulse formation was initiated and stabilized by nonlinear polarization evolution (NPE). Acting as a fast artificial saturable absorber (ASA), NPE relies on the coherent addition of the right- and left- circularly polarized optical waves propagating inside single-mode fiber (SMF). The primary advantage of NPE is its near-instantaneous response and strong modulation depth (the difference in unsaturated and saturated loss). In addition, NPE is a natural choice for fiber oscillators as the long lengths of SMF allow for large $\chi^{(3)}$ nonlinear processes.

Experiments on femtosecond fiber oscillators reported in Chapters 1 through 4 indicate that NPE provides an upper limit to pulse energy. Because of its interferometric action, it is possible to overdrive NPE at high energies. This results in decreasing transmission with pulse energy (Figure 1.4) and leads to pulse breakup. Another disadvantage of NPE in fiber lasers is that it necessitates the use of SMF which is prone to stress-induced birefringence. This results in reduced environmental stability. The use of polarization-maintaining (PM) fiber leads to improved environmental stability; however, it precludes NPE pulse shaping.

In comparison to modelocked solid-state lasers, ultrafast fiber lasers have historically traded pulse energy for increased stability. The possibility of producing high-energy (10's of nJ's) and short-duration (< 100-fs) pulses from an environmentally stable, compact, and inexpensive source could revolutionize the rapidly growing commercial market for femtosecond sources. Consequently, there is strong motivation to study alternative saturable absorbers inside fiber lasers.

One alternative is to modelock a fiber laser with a semiconductor saturable absorber. In this case, the saturable absorber action is the result of optically induced energy transitions within a semiconductor crystal. At high light intensities, these transitions bleach or saturate, causing the light absorption to decrease.

Saturable absorption in semiconductors occurs through two mechanisms. Transitions between the valence and conduction bands, called interband transitions, occur on a nanosecond to picosecond time scale depending upon how the semiconductor material is grown. Intraband carrier-carrier scattering and thermalization processes occur on a much faster time scale, typically 10 to 100 femtoseconds. When used to modelock a laser, the slow bleaching process promotes the formation of a pulse from noise while the fast bleaching helps to stabilize modelocked operation.

The advantage of using a semiconductor saturable absorber as opposed to an ASA is that the former cannot be overdriven in the same sense that the latter can (For example, Figure 1.4 in Chapter 1 shows a typical NPE transmission

curve with the overdriven regions). One disadvantage is that the interband transitions (the strongest component to saturable absorption) are relatively slow. This tends to produce longer pulse durations. Another potential problem is that the semiconductor material is prone to optical damage at very high intensities.

Semiconductor saturable absorbers are typically packaged as semiconductor saturable absorber mirrors (SESAM's). The saturable absorber is encased within a Fabry-Perot cavity formed by a semiconductor Bragg mirror on the bottom and a dielectric mirror on the top (on the reflecting side). This is shown schematically in Figure 6.1. Other designs tend to be variations on this.

Figure 6.1 A typical SESAM design. The absorber is sandwiched between two high reflectors.

An excellent review of SESAM's in modelocked lasers is given by Keller *et. al.* [1]. SESAM's have been used successfully to modelock solid-state lasers, and numerous examples exist in the literature. For example, two-cycle

pulses were generated from a Ti:sapphire laser using Kerr-lens modelocking assisted by a SESAM [2]. Less work has been reported using SESAM's in fiber lasers. A recent experiment reports self-similar operation in an all-PM Yb-doped fiber laser modelocked with a SESAM [3]. The results are very encouraging; however, the pulse energy was limited to ~ 1 nJ, countering the main practical benefit of a self-similar fiber laser.

In this chapter, a Yb fiber laser is modelocked with a SESAM, producing femtosecond pulses with the potential for attaining several nJ's of energy. The laser appears to favor self-similar evolution as reported in Reference [3]. At large normal GVD, the laser produces chirped-pulse evolution as observed in Chapter 4 with a fiber laser modelocked by NPE. The resulting pulse energy is ~ 2 nJ, limited by large intra-cavity losses. A better laser architecture which would incorporate a transmitting semiconductor saturable absorber is expected to produce higher pulse energies.

6.2 Fiber laser setup

The basic fiber laser setup is shown in Figure 6.2. This is a modification to the ring geometry which includes a linear segment in the open-air section. The SESAM is placed at the end of the linear segment. This architecture is often referred to as a sigma cavity. A sigma design is chosen over a linear cavity because the former is closer in architecture to a ring cavity, which is known to produce stable, high-energy femtosecond pulses. The second half wave plate (labeled "HWP2" in Figure 6.2) is set to direct light through the second beam cube (labeled "BC2") onto the SESAM. The second quarter wave plate

(labeled “QWP2”) is set to direct light reflected off the SESAM into the dispersive delay line. An open-air isolator makes the laser unidirectional with light traveling counterclockwise in the figure.

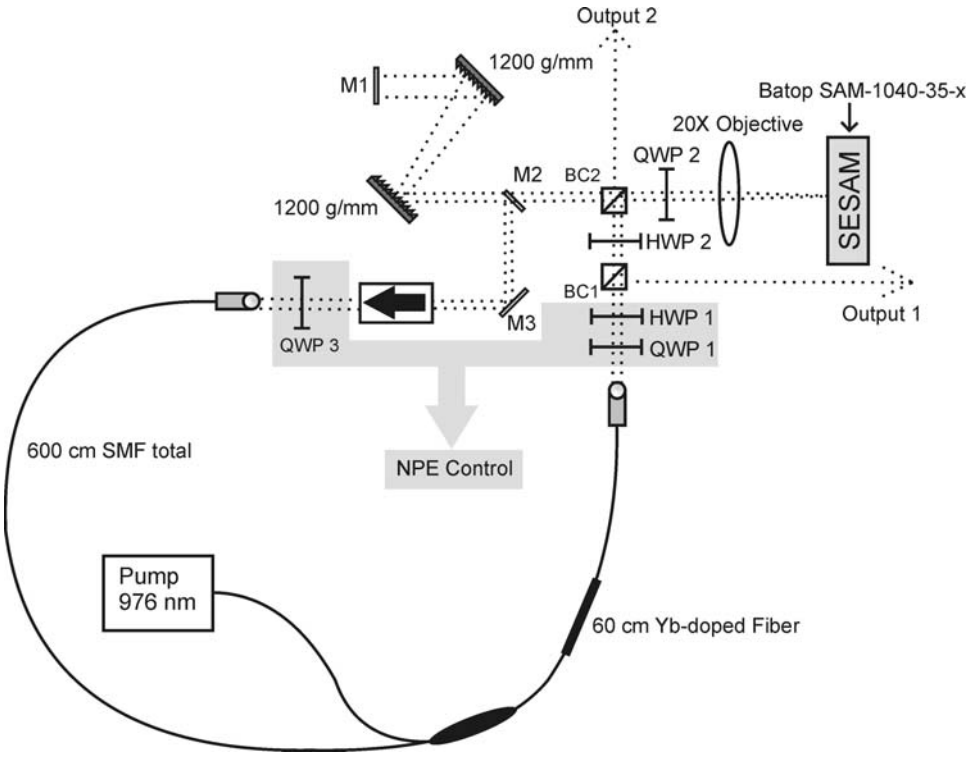

Figure 6.2 Yb fiber laser setup. QWP: quarter wave plate. HWP: half wave plate. BC: polarizing beam cube. M: mirror.

The SESAM was manufactured at Batop Optoelectronics. It is spectrally centered at 1040 nm with a very broad ~120-nm bandwidth. The non-saturable loss is < 5 %. The saturable absorbance is 35 % at the center wavelength. The saturation fluence is 70 $\mu J/cm^2$, and the slow relaxation time is < 10 ps. A 20x microscope objective is used to focus light onto the SESAM. The resulting fluence is roughly 5 to 10 times the saturation fluence assuming 1-nJ pulses.

Initially, NPE was used in combination with the SESAM to modelock the laser. NPE was controlled with two quarter wave plates, one half wave plate, and a polarizing beam cube. This is shown schematically in Figure 6.2 as the shaded region. Once it was determined that the laser would modelock, NPE control (the shaded region in Figure 6.2) was removed.

In the absence of NPE, the laser is modelocked by translating the SESAM through the focal plane of the 20x microscope objective. Because non-PM fiber is used in this experiment, some residual NPE action likely exists in the fiber. However, without control, it is highly unlikely that this residual NPE is biased correctly to modelock the laser by itself. Different modelocked spectra are generated simply by perturbing the SESAM. A strong tendency to multi-pulse is observed when the 20x objective is replaced with a 40x objective. This is expected when the fluence is much greater than the saturation fluence of the SESAM (Reference [1]). These observations convince us that the SESAM contributes strongly to pulse formation.

Unfortunately, the sigma cavity design is particularly difficult to align owing to the retro-reflection occurring at the SESAM. In order to modelock the laser, the SESAM must be translated into and out of focus. This results in reduced beam collimation and effectively misaligns the laser. One potential solution to this problem is to incorporate the design shown in Figure 6.3 in which a parallel mirror-SESAM combination is placed inside a telescope. To modelock the laser, the mirror-SESAM pair is translated through the focal plane of the telescope.

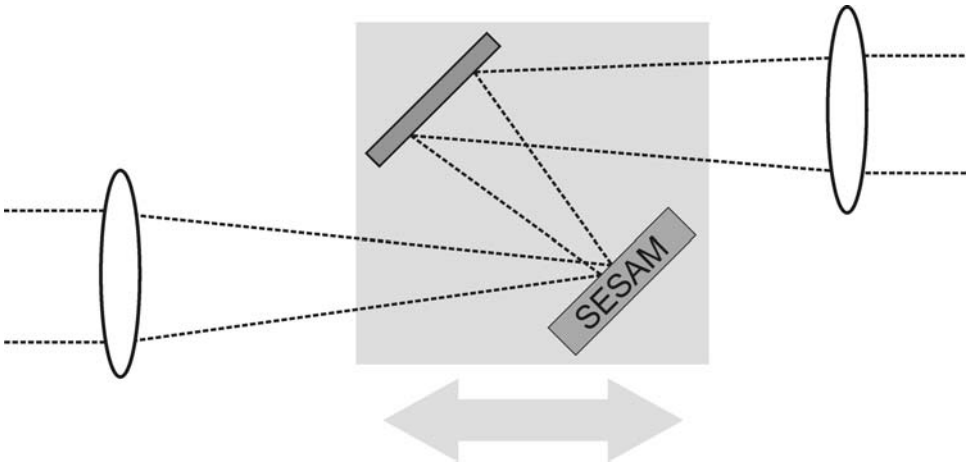

Figure 6.3 A SESAM configuration that fits within a ring cavity.

This configuration has two advantages. First, the output beam remains collimated as the mirror-SESAM pair is translated through the focal plane. Second, this design can be incorporated inside a ring cavity which is expected to be more stable than a sigma cavity. Perhaps an even better design is to incorporate a transmission semiconductor saturable absorber directly into a ring cavity. Future work should implement these designs in experiment.

6.3 Experimental results

Using only the SESAM to modelock the laser, pulsed operation is explored at different net cavity group velocity dispersion (GVD), achieved by varying the separation between the intra-cavity diffraction gratings. Admittedly, the laser is very difficult to modelock and sensitive to slight misalignments. This limits our exploration to a relatively narrow range of normal GVD, where we observed the best performance. Figure 6.4 illustrates typical data taken at a net GVD of 0.035 +/- 0.002 ps^2. Figure 6.4(a) shows the modelocked spectra rejected (solid line) and accepted (dashed line) from the first output port

("BC1" in Figure 6.2). As discussed in Chapter 4, the qualitative resemblance between these two spectra illustrates the lack of NPE action which is expected in this case. Figure 6.4(b) shows the measured interferometric autocorrelation (AC) of the dechirped pulse and the chirped-pulse AC as an inset. The pulses are very highly chirped coming from BC1, and the resulting chirped-pulse AC extends beyond the dynamic range of the autocorrelation measurement. As a result, the chirped-pulse AC is calculated from the measured dechirped AC. The chirped pulse duration is inferred to be ~ 9 ps. The chirped pulse energy is 2.1 nJ, limited by large loss in the open-air section.

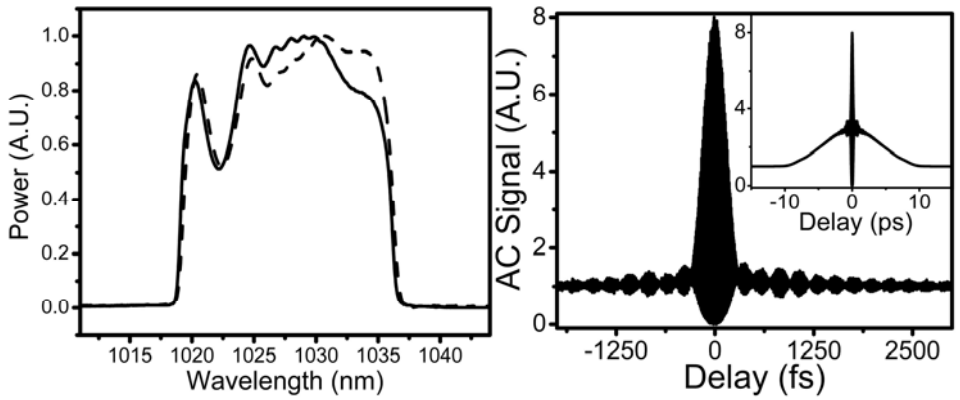

Figure 6.4 (a) Spectra rejected (solid line) and accepted (dashed line) from BC1. (b) Measured AC of dechirped pulse and calculated AC of the chirped pulse (inset).

The intensity and phase of the dechirped pulse is inferred using a pulse retrieval algorithm based on fitting the measured interferometric autocorrelation and spectrum [4]. Figure 6.5 shows the result of this fit. The inferred pulse intensity is quite structured with some phase modulation across the main pulse. The dechirped duration is measured to be ~ 200 fs full-width-at-half-maximum (FWHM), which is about 55% beyond transform limit.

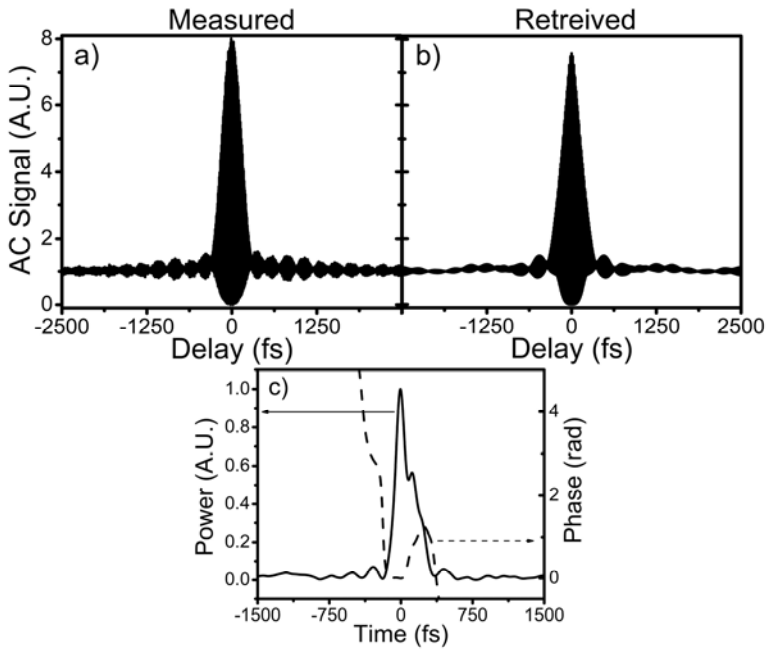

Figure 6.5 (a) Measured autocorrelation of dechirped pulse. (b) Calculated autocorrelation of retrieved pulse. (c) Retrieved pulse intensity (solid) and phase (dashed) profiles.

It is interesting to compare this modelocked operation to a similar fiber laser modelocked only with NPE (reported in Chapters 2 through 5). Figure 6.6 compares modelocked spectra at different cavity GVD. The left column of the figure [Figure 6.6(a)-(c)] corresponds to the SESAM laser shown in Figure 6.2. The right column [Figure 6.6(d)-(f)] corresponds a similar laser which uses NPE as a saturable absorber. Qualitatively, the spectra are similar, although the NPE laser shows greater variation in bandwidth as a function of GVD.

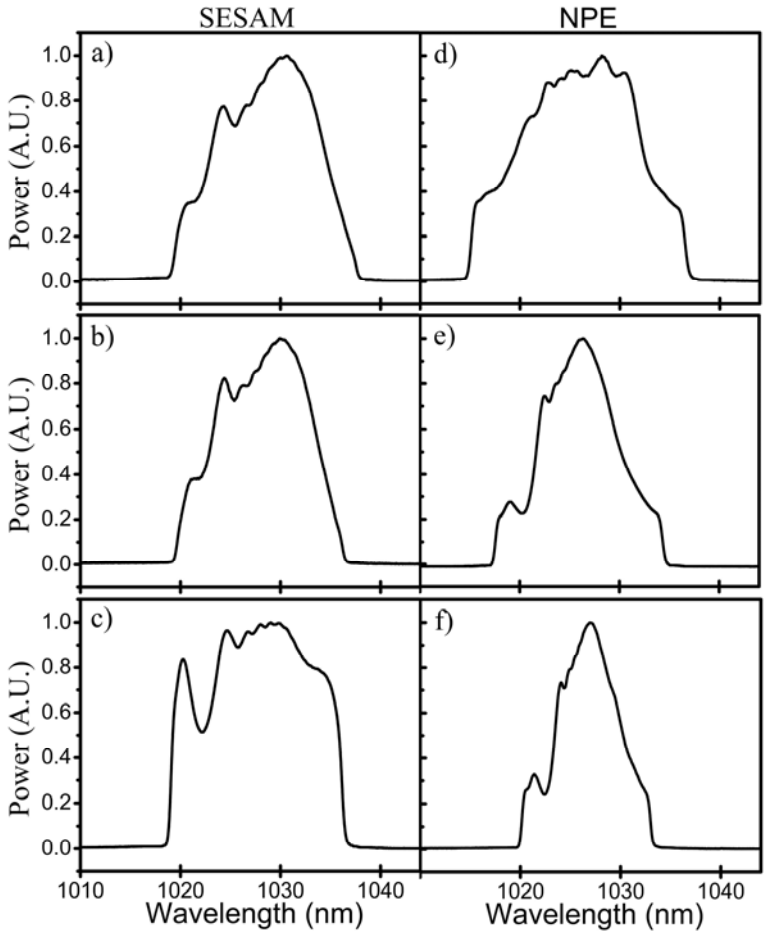

Figure 6.6 [(a)-(c)] modelocked spectra from SESAM laser. (a) GVD = 0.016 ps^2. (b) GVD = 0.022 ps^2. (c) GVD = 0.035 ps^2. [(d)-(f)] modelocked spectra from an NPE laser. (d) GVD = 0.015 ps^2. (e) GVD = 0.028 ps^2. (f) GVD = 0.036 ps^2.

Figure 6.7 compares laser performance versus net GVD for the SESAM laser and a similar laser using NPE. Figure 6.7(a) shows the FWHM duration of the chirped output pulses. Figure 6.7(b) shows the spectral bandwidth of the output pulses. Figure 6.7(c) shows the pulse quality as measured by comparing the pulse to its transform-limited duration. Figure 6.7(d) shows the FWHM duration of the dechirped pulses. In this figure, the solid spheres represent the SESAM laser, and the triangles represent an NPE laser.

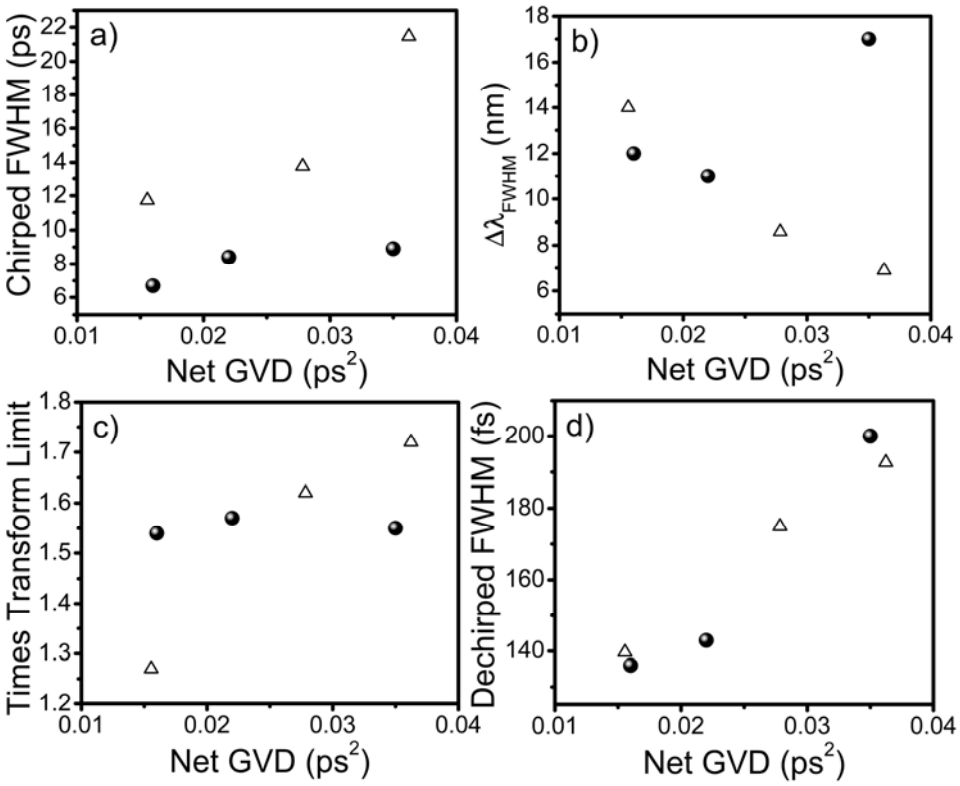

Figure 6.7 (a) Duration of chirped output pulses. (b) Spectral bandwidth. (c) Pulse quality. (d) Duration of dechirped output pulses. In all figures, the triangles correspond to the laser modelocked with NPE and the spheres correspond to the SESAM laser.

The same qualitative trends with increasing GVD are seen between the two lasers. One interesting difference is in the chirped pulse duration [Figure 6.7(a)]. The SESAM laser produces shorter chirped pulses than the NPE laser at all measured GVD values. One possible explanation for this is that the NPE laser requires highly chirped pulses at large normal GVD in order to assist NPE action through spectral filtering in the gain. This observation was mentioned in Chapter 3 for the chirped-pulse oscillator.

Another interesting point is that the bandwidth and pulse quality generated from the two lasers are comparable with the one exception of the data taken at

0.035 ps^2. Consequently, the dechirped pulses are similar in duration. It should be emphasized that the SESAM laser is capable of producing 100- to 200-fs pulses even though the slow response of the SESAM is on the order of 10 ps. The exact mechanism for generating femtosecond pulses is not known. Soliton pulse-shaping is not expected to be strong at net normal GVD. Perhaps the fast response of the SESAM coupled with gain filtering is enough to shape and stabilize femtosecond pulses.

The intra-cavity breathing ratio (inferred from the calculated chirped-pulse AC's) is shown in Figure 6.8.

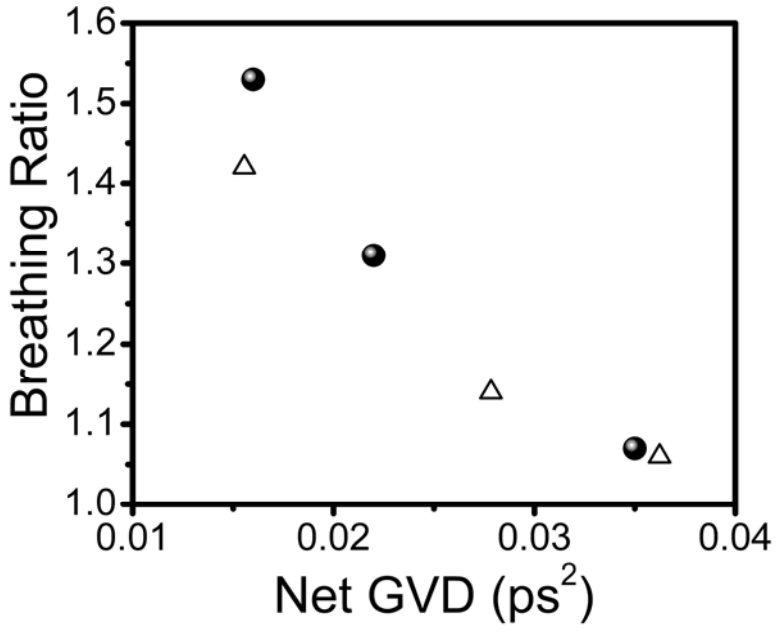

Figure 6.8 Intra-cavity breathing ratio. Triangles = NPE laser. Spheres = SESAM laser.

Not only does the SESAM laser closely follow the NPE laser trend, but it also produces almost static pulses at large normal GVD. As mentioned in Chapter 3,

this mode of operation is a limit of self-similar evolution at large normal GVD. No other type of pulse evolution is observed with the SESAM laser. For some reason, it seems to prefer self-similar operation. This was also observed in Reference [3].

6.4 Conclusions and acknowledgements

In conclusion, we demonstrate the operation of a Yb fiber laser modelocked with a SESAM. Self-similar and chirped-pulse evolution are observed in the laser, and 100- to 200-fs pulses can be generated. The laser is capable of producing 2-nJ pulse energy. The pulse energy is believed to be limited by large loss in the open-air section of the cavity. Better laser architecture (for example, using a transmission semiconductor saturable absorber) should greatly improve the performance of the laser. This laser represents a first step toward a more integrated, high-energy femtosecond fiber source.

Portions of this work were supported by the NIH, and NSF-ECS. This work was performed with the assistance of Andy Chong. Special thanks go to Max Stumpf who conceived the SESAM design shown in Figure 6.3.

BIBLIOGRAPHY

[1] U. Keller, K.J. Weingarten, F.X. Kärtner, D. Kopf, B. Braun, I.D. Jung, R. Fluck, C. Hönninger, N. Matuschek, and J. Aus der Au, "Seimiconductor Saturable Absorber Mirrors (SESAM's) for Femtosecond to Nanosecond Pulse Generation in Solid-State Lasers," IEEE J. Selected Topics Quant. Elec. **2**, 435 (1996).

[2] D.H. Sutter, G. Steinmeyer, L. Gallmann, N. Matuschek, F. Morier-Genoud, U. Keller, V. Scheuer, G. Angelow, and T. Tschudi, "Semiconductor saturable-absorber-mirror-assisted Kerr-lens-mode-locked Ti:sapphire laser producing pulses in the two-cycle regime," Opt. Lett. **24**, 631 (1999).

[3] C.K. Nielson, B. Ortac, T. Schreiber, J. Limpert, R. Hohmuth, W. Richter, and A. Tünnermann, "Self-starting self-similar all-polarization maintaining Yb-doped fiber laser," Opt. Exp. 13, 9346 (2005).

[4] J.W. Nicholson, J. Jasapara, and W. Rudolph, "Full-field characterization of femtosecond pulses by spectrum and cross-correlation measurements," Opt. Lett. **24**, 1774 (1999).

Chapter 7

Future directions

A continuation of the work discussed in this thesis will improve our understanding of the limitations to achieving higher pulse energies and shorter pulse durations from femtosecond fiber oscillators. To better understand the physics behind femtosecond fiber lasers, it will be necessary to develop a successful analytic theory such as has been achieved for solid-state lasers [1,2]. In the meantime, our intuition will continue to be guided by numerical simulation. Numerical simulations presented in this thesis are the result of solving a one-dimensional nonlinear Schrödinger equation. Obviously, better insight will come from solving the coupled equations in three dimensions.

A direct measurement of nonlinear polarization evolution (NPE) in fiber lasers would be very valuable. Such a measurement is not trivial since NPE is directly linked to the pulse evolution inside the cavity. Consequently, attempts to directly measure NPE usually change the performance of the laser being measured. One possible way to measure NPE would be to couple a pulse from a probe laser into the "cold" (i.e. not lasing) cavity of a test laser.

With the goal of achieving higher pulse energy from femtosecond fiber lasers, two approaches are very promising. Given that NPE appears to be the primary limitation, further work needs to be done with SESAM-based fiber oscillators. SESAM technology is now sufficiently advanced that standard products are available for a range of center wavelengths, bandwidths, and

modulation depths. Also, the response times are now just a few picoseconds. Based on the results of Chapter 6, a transmission semiconductor saturable absorber could likely replace NPE in a fiber ring laser, allowing for the generation of femtosecond pulses. High pulse energies should be possible without over-saturating the SESAM [3].

The second promising approach to achieving high energy is to utilize double-clad fiber geometry. Double-clad gain fiber (for example, Yb-doped fiber) allows for the absorption of several Watts of pump power into the fiber core. Recently, some encouraging results have been reported with double-clad Yb-doped fiber lasers [4,5].

With regard to achieving shorter pulse durations, it will be necessary to fully compensate 3^{rd}- and possibly 4^{th}-order dispersion in fiber, as well as to reduce excessive fiber nonlinearities. One interesting approach would be to incorporate a spatial light modulation (SLM) inside the dispersive delay line of a fiber laser. A programmable voltage is applied across a one-dimensional array of liquid crystal cells which, in turn, modulate the phase of a spectrally dispersed beam. Although using an SLM would detract from some of the integration of fiber oscillators, in theory, one could exactly cancel any phase distortions which arise during propagation in single-mode fiber (SMF).

With regard to stability, fiber lasers will ultimately become polarization maintaining (PM) in order to avoid stress-induced instabilities. A SESAM laser such as is reported in Chapter 6 should be less susceptible to environmental instabilities as it would only possess a weak residual NPE. By

replacing all the SMF with PM fiber, the resulting laser should be entirely stable against environmental stresses. Some progress has been made in achieving such a stable fiber laser [6].

Partially due to work presented in this thesis, Yb-doped fiber lasers are directly competitive with solid-state lasers at key wavelengths. Long-term stability, an integrated design, and reduced cost are the primary reasons that ultrafast fiber lasers are at the forefront of a rapidly growing commercial market for femtosecond sources. Much work remains to be done to improve the performance of short-pulse fiber oscillators. Our understanding continues to develop, and ultrafast fiber lasers offer many opportunities for rewarding scientific research.

BIBLIOGRAPHY

[1] H. A. Haus, J. G. Fujimoto, and E. P. Ippen, "Analytic theory of additive pulse and Kerr lens mode locking," IEEE J. Quantum Electron. **28**, 2086 (1992).

[2] H.A. Haus, J.G. Fujimoto, and E.P. Ippen, "Structures for additive pulse mode locking," J. Opt. Soc. Am. B **8**, 2068 (1991).

[3] U. Keller, K.J. Weingarten, F.X. Kärtner, D. Kopf, B. Braun, I.D. Jung, R. Fluck, C. Hönninger, N. Matuschek, and J. Aus der Au, "Seimiconductor Saturable Absorber Mirrors (SESAM's) for Femtosecond to Nanosecond Pulse Generation in Solid-State Lasers," IEEE J. Selected Topics Quant. Elec. **2**, 435 (1996).

[4] A. Albert, V. Coudec, L. Lefort, A. Barthelemy, "High-energy femtosecond pulses from an ytterbium-doped fiber laser with a new cavity design," IEEE P. Tech. Lett. **16**, 416 (2004).

[5] M.J. Messerly, J.W. Dawson, and C.P.J. Barty, "25 nJ Passively Mode-Locked Fiber Laser at 1080 nm," Conference on Lasers and Electro-Optics (CLEO), CThC7, Long Beach, CA (2006).

[6] C.K. Nielson, B. Ortac, T. Schreiber, J. Limpert, R. Hohmuth, W. Richter, and A. Tünnermann, "Self-starting self-similar all-polarization maintaining Yb-doped fiber laser," Opt. Exp. 13, 9346 (2005).